# ORIGINAL RESEARCH

The *CEL-HYB1* Hybrid Allele Promotes Digestive Enzyme Misfolding and Pancreatitis in Mice

Xiao-Tong Mao, MD,[1,2,*] Wen-Bin Zou, MD,[1,2,*] Yu Cao, MD,[1,2,*] Yuan-Chen Wang, BM,[1,2]
Shun-Jiang Deng, BM,[2] David N. Cooper, PhD,[3] Claude Férec, MD, PhD,[4]
Zhao-Shen Li, MD,[1,2] Jian-Min Chen, MD, PhD,[4,§] and Zhuan Liao, MD[1,2,§]

[1]Department of Gastroenterology, Changhai Hospital, The Second Military Medical University, Shanghai, China; [2]Shanghai Institute of Pancreatic Diseases, Shanghai, China; [3]Institute of Medical Genetics, School of Medicine, Cardiff University, Cardiff, United Kingdom; and [4]Univ Brest, Inserm, EFS, UMR 1078, GGB, F-29200 Brest, France
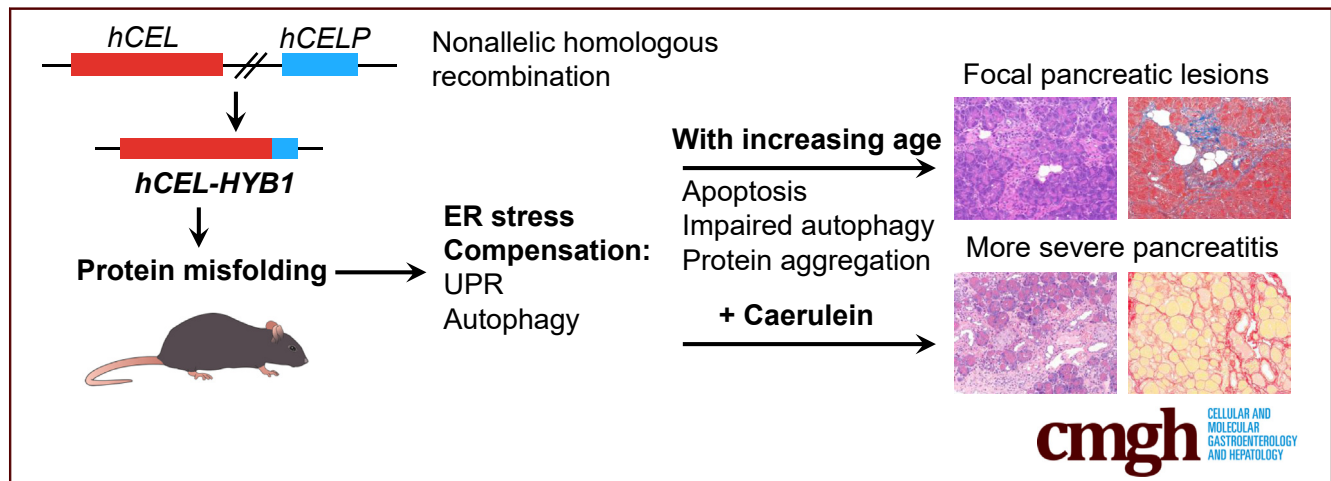
SUMMARY

The hybrid allele of the carboxyl ester lipase gene (CEL-HYB1) increases the risk of chronic pancreatitis. Here, we report that expression of a humanized form of CEL-HYB1 in mice promotes pancreatitis through protein misfolding, endoplasmic reticulum stress, and impaired autophagy.

BACKGROUND & AIMS: A hybrid allele that originated from homologous recombination between *CEL* and its pseudogene (*CELP*), *CEL-HYB1* increases the risk of chronic pancreatitis (CP). Although suggested to cause digestive enzyme misfolding, definitive in vivo evidence for this postulate has been lacking.

METHODS: CRISPR-Cas9 was used to generate humanized mice harboring the *CEL-HYB1* allele on a C57BL/6J background. Humanized *CEL* mice and C57BL/6J mice were used as controls. Pancreata were collected and analyzed by histology, immuno-histochemistry, immunoblotting, and transcriptomics. Isolated pancreatic acini were cultured in vitro to measure the secretion and aggregation of CEL-HYB1 protein. Mice were given caerulein injections to induce acute pancreatitis (AP) and CP.

RESULTS: Pancreata from mice expressing CEL-HYB1 developed pathological features characteristic of focal pancreatitis that included acinar atrophy and vacuolization, inflammatory infiltrates, and fibrosis in a time-dependent manner. CEL-HYB1 expression in pancreatic acini led to decreased secretion and increased intracellular aggregation and triggered endoplasmic reticulum stress compared with CEL. The autophagy levels of pancreata from mice expressing CEL-HYB1 changed at different developmental stages; some aged *CEL-HYB1* mice exhibited an accumulation of large autophagic vesicles and impaired autophagy in acinar cells. Administration of caerulein increased the severity of AP/CP in mice expressing CEL-HYB1 compared with control mice, accompanied by higher levels of endoplasmic reticulum stress.

CONCLUSIONS: Expression of a humanized form of CEL-HYB1 in mice promotes endoplasmic reticulum stress and pancreatitis through a misfolding-dependent pathway. Impaired autophagy appears to be involved in the pancreatic injury in aged *CEL-HYB1* mice. These mice have the potential to be used as a model to identify therapeutic targets for CP. *(Cell Mol Gastroenterol Hepatol 2022;14:55–74; https://doi.org/10.1016/j.jcmgh.2022.03.013)*

Chronic pancreatitis (CP) is a multifactorial, inflammatory syndrome of the pancreas that leads to extensive fibrotic tissue replacement and exocrine/endocrine pancreatic insufficiency.[1] Based upon observations of

pancreatic autolysis in autopsy studies, Chiari suggested some 125 years ago that pancreatitis was an autodigestive disease resulting from the premature activation of trypsinogen in the pancreas.[2] Over the past 25 years, this trypsin-centered theory of pancreatitis has received strong support from the discovery of a steadily growing list of CP-related genetic risk variants that perturb the balance between the activation and inhibition of trypsin in the pancreas.[3] These include (1) both qualitative and quantitative gain-of-function variants in the *PRSS1* gene (encoding cationic trypsinogen),[4-7] (2) loss-of-function variants in the *SPINK1* (encoding pancreatic secretory trypsin inhibitor)[8,9] and *CTRC* (encoding chymotrypsin C that promotes trypsinogen degradation)[10] genes, and (3) an inversion at the chymotrypsin B1-B2 (*CTRB1-CTRB2)* locus that affects protective trypsinogen degradation.[11,12] In addition, a degradation-sensitive missense variant in the *PRSS2* gene (encoding anionic trypsinogen)[13] has been found to protect against pancreatitis. More recently, a protein misfolding-dependent pathway was identified as an additional and quite distinct pathological mechanism that drives the development of pancreatitis.[14,15] Specifically, a subset of pancreatitis-related *PRSS1* variants had no impact on trypsin activity, but instead caused enzyme misfolding and endoplasmic reticulum (ER) stress in cell culture.[16,17] In vitro and in vivo studies of the pathogenic *CPA1* N256K missense substitution also provided convincing evidence that mutation-induced enzyme misfolding can lead to progressive CP via an ER stress-related mechanism.[18,19]

A hybrid allele that originated from homologous recombination between *CEL* and its tandemly arranged pseudogene (*CELP*), originally termed *CEL-HYB* and now known as *CEL-HYB1*, was found to be over-represented in 3 European cohorts with nonalcoholic CP as compared with healthy controls (pooled odds ratio, 5.2).[20] *CEL-HYB1* exhibited ethnic differences in frequency as it was found to be absent in 3 Asian populations.[21] A different hybrid allele, also involving *CEL* and *CELP,* and termed *CEL-HYB2*, has been identified in Asian populations but it is not associated with CP. Interestingly, mRNA analysis in transfected cells demonstrated that the *CEL-HYB2* transcript was significantly degraded by nonsense-mediated mRNA decay in contrast to the *CEL-HYB1* transcript.[21] Moreover, a recent study analyzed the *CEL-HYB1* allele in Polish children with CP; although the *CEL-HYB1* allele was more frequent in patients with CP (4.8%) than in controls (2.4%), the difference was not statistically significant.[22] It should, however, be noted that the carrier frequency of *CEL-HYB1* in Polish healthy controls[22] was rather higher than in Germany (0.7%-1.0%), France (0.7%) and Norway (0.5%).[20]

The *CEL* gene comprises 11 exons. In the *CEL-HYB1* allele, the last exon of *CEL* is replaced by exon 11′ of *CELP*.[20] Consequently, the difference between the wild-type CEL protein and the mutant CEL-HYB1 protein lies in the carboxyl terminal amino acid sequence. In this regard, exon 11 of *CEL* contains a 33-bp variable number tandem repeat (VNTR) region that encodes a series of repetitive 11-amino acid segments. The number of VNTR repeats is polymorphic, fluctuating from 3 to 23, with 16 repeats being the most

common.[23,24] Replacement of *CEL* exon 11 by *CELP* exon 11′ introduces a premature stop codon within the third VNTR, thereby removing virtually all of the repetitive 11-amino acid segments that are normally present at the carboxyl terminal end of CEL. It should be noted that single base-pair deletions in the VNTR region (generating a frameshift), which induce a novel truncated C-terminus, can cause a dominantly inherited syndrome of exocrine dysfunction and diabetes.[25]

Previous studies have demonstrated that the *CEL-HYB1* variant elicits enzyme misfolding, protein aggregation and ER stress in transfected human embryonic kidney (HEK) 293T cells.[20,26,27] However, the *CEL-HYB1* variant has no impact on lipase activity, and *Cel*-knockout mice do not develop obvious lesions in the pancreas.[26,28] These findings suggest that the impact of *CEL-HYB1* is not due to the loss of CEL protein or activity per se, but rather to the misfolding-dependent pathway of genetic CP risk. However, to date, in vivo evidence demonstrating the pathogenicity of the *CEL-HYB1* allele has been lacking. Herein, we report the generation and functional characterization of humanized *CEL-HYB1* and *CEL* mice.

Results

Generation of hCEL-HYB1 and hCEL Mouse Strains

The aim of this study was to assess the pathological impact of the CEL-HYB1 fusion protein in mouse pancreas. To this end, we generated 2 humanized mouse strains harboring the *CEL-HYB1* risk allele and the wild-type human *CEL* gene (ie, *hCEL-HYB1* and *hCEL* mice) using CRISPR/Cas9 gene editing. To facilitate observation of the CEL and CEL-HYB1 proteins, we added a 3×Flag epitope tag at the amino terminus of the CEL or CEL-HYB1. Then, to determine whether the Flag tag might affect CEL-HYB1 protein misfolding, we transfected the plasmids expressing CEL or CEL-HYB1 with or without a Flag tag into HEK293T cells in vitro. We found that there were no significant differences between CEL-HYB1 with and without a Flag tag in terms of protein secretion and aggregation (Figure 1A, B), or misfolding-induced ER stress (Figure 1C, D, E).

Donor vector containing the *hCEL-HYB1* exon2～11-3×Flag-*mCel* 3′UTR-polyA frame or the *hCEL* exon2～11-
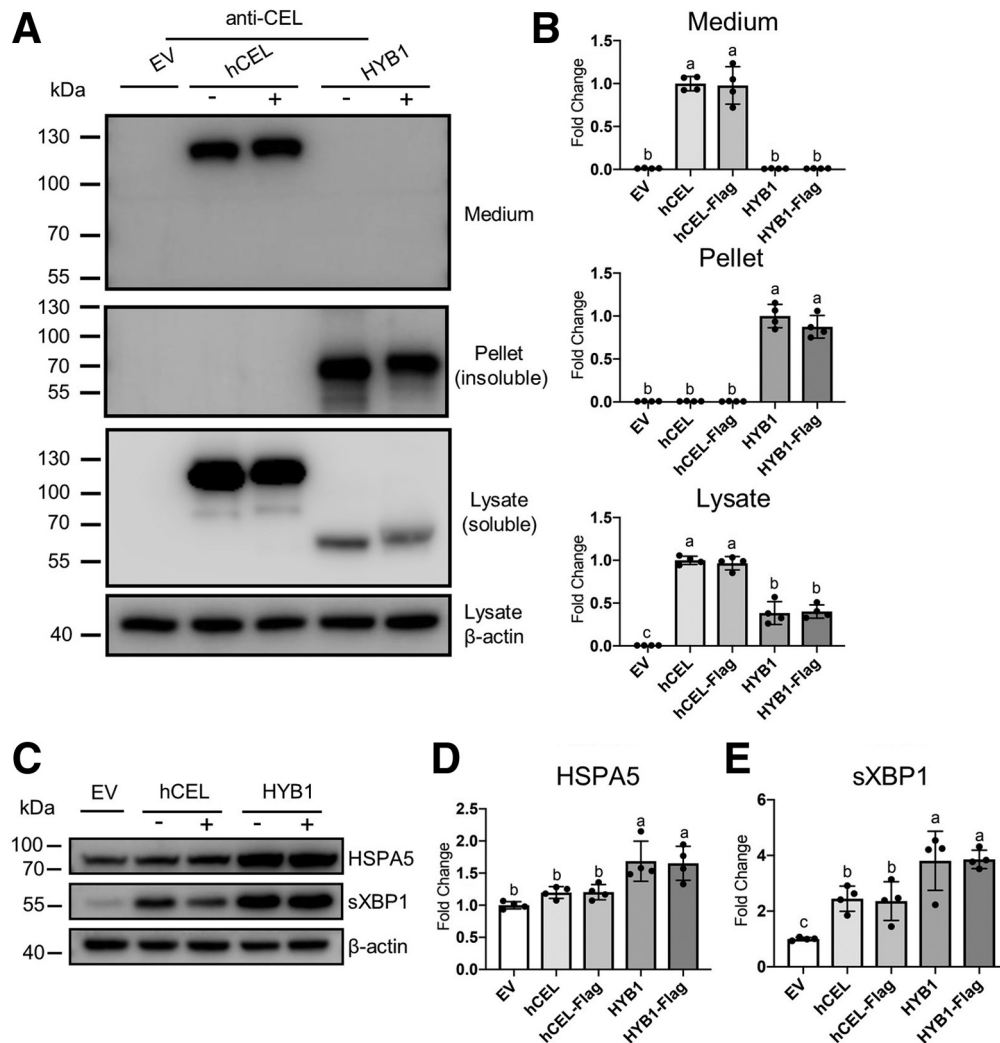
Most current article

Figure 1. Expression of tagged and untagged wild-type hCEL and CEL-HYB1 in HEK293T cells. HEK293T cells were transiently transfected with plasmids encoding wild-type hCEL and CEL-HYB1 with or without a 3×Flag tag (+/−). (*A*) Cell medium and soluble (lysate) and insoluble (pellet) fractions were harvested after 48 hours and were analyzed by Western blotting. Each blot is representative of 4 independent experiments. Empty vector (EV) (negative control). β-actin was measured as a loading control. (*B*) Quantification of Western blot band intensities adjusted to the β-actin levels. (*C*) Expression of ER stress markers HSPA5 and sXBP1 were assessed by Western blotting of the soluble (lysate) fractions. (*D* and *E*) Quantification of marker band intensities after adjustment to the β-actin levels and normalization to the expression in EV-transfected cells. Throughout the Figure, data are presented as mean values ± standard deviation (*SD*) (n = 4); bars with different letters represent significant differences in means by 1-way analysis of variance with Sidak's multiple comparisons.

3×Flag-*mCel* 3′UTR-polyA frame (Figure 2*A*) was used to introduce the targeting sequence into the mouse genome in fertilized C57BL/6J eggs. As illustrated in Figure 2*B*, the *hCEL-HYB1* or *hCEL* open reading frame was inserted into exon 2 of the mouse *Cel* gene by homology-directed repair. As such, the expression of the *hCEL-HYB1* or *hCEL* open reading frame is placed under the physiological control of the mouse *Cel* gene's upstream regulatory sequence. Moreover, since exon 1 encodes the signal peptide, the secretion of hCEL-HYB1 or hCEL will be guided by the murine signal peptide sequence (Figure 2*C*). Further, since the proximal portion of mouse *Cel* exon 2 that was unaltered during homology-directed repair has an identical nucleotide sequence to human *CEL*, the mature hCEL-HYB1 or hCEL

protein does not contain any mouse-specific protein sequence. Finally, the transgenic expression of *hCEL-HYB1* or *hCEL* would simultaneously silence the expression of the endogenous murine *Cel* gene. Indeed, the hCEL-HYB1 and hCEL proteins were successfully expressed in the corresponding transgenic mouse pancreas, as confirmed by Western blot and immunohistochemistry (Figure 2*D*, *E*). As expected, we did not detect mouse Cel protein expression in the pancreas of these 2 knock-in mouse strains. It should be noted that the mouse Cel protein has a much lower molecular weight than its human counterpart due to it containing only 3 of the repetitive 11-amino acid segments at the carboxyl terminus.[29] Although the expression of *hCEL-HYB1* or *hCEL* is under the physiological control of the
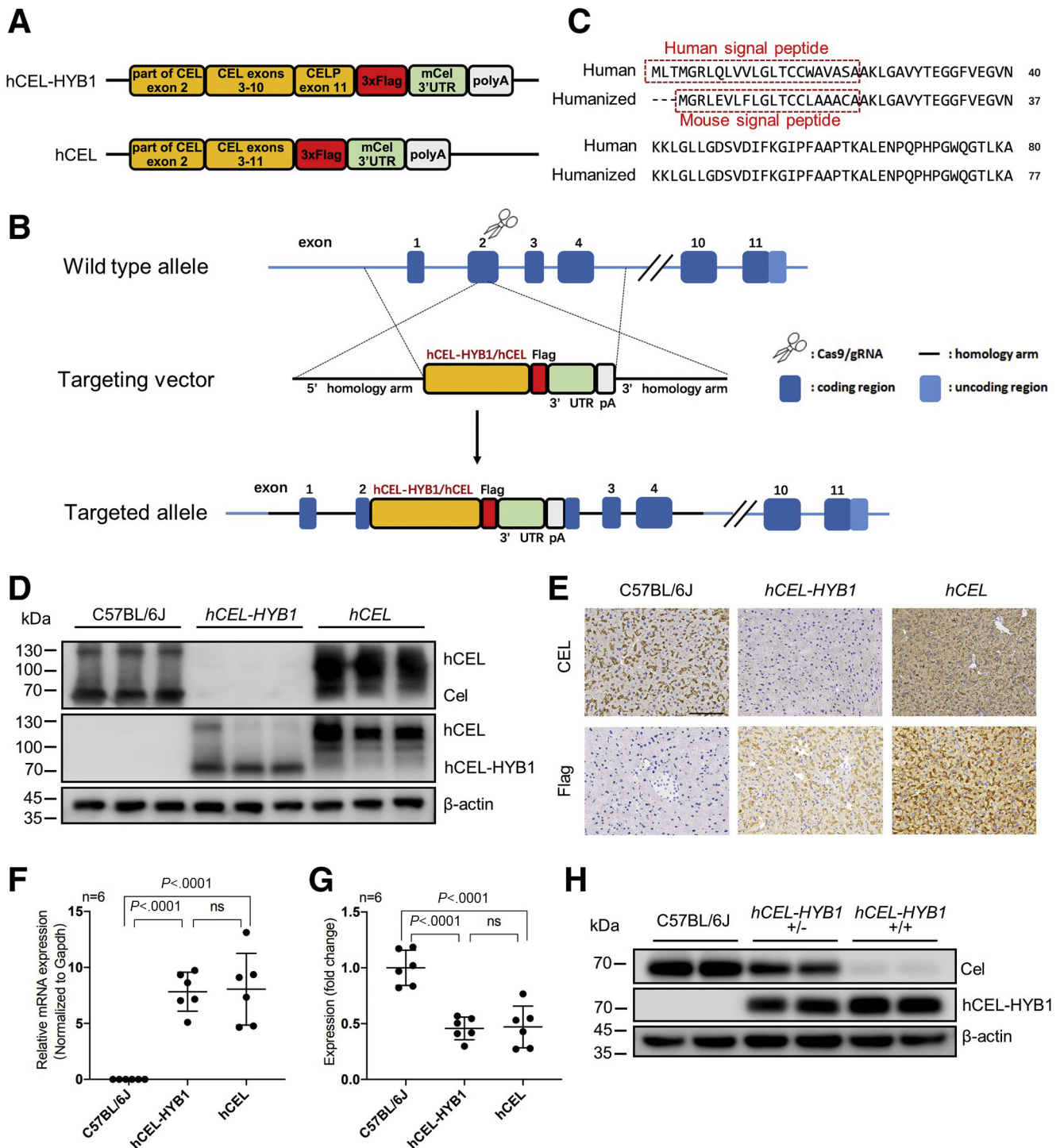
Figure 2. Generation of humanized carboxyl ester lipase (*CEL*) mice and expression analysis. (*A*) Targeting sequences (containing Flag tag) were designed for developing humanized *CEL* or *CEL-HYB1* mice and (*B*) inserted into exon 2 of mouse *Cel* separately by CRISPR/Cas9 gene editing. (*C*) The signal peptide of CEL protein expressed by humanized mice is derived from mouse *Cel*. (*D*) Expression of CEL protein in the soluble fraction from mice aged 12 weeks was detected by Western blot analysis using anti-CEL (*upper*) and anti-Flag antibodies (*middle*). β-actin was measured as a loading control (*down*). (*E*) Immunohistochemical analysis of CEL protein expression in the pancreata of C57BL/6J, *hCEL-HYB1*, and *hCEL* mice. Scale bar = 100 μm. (*F*) Pancreatic mRNA expression of mouse *Cel*, *hCEL-HYB1*, and *hCEL* using a primer pair specific for *hCEL-HYB1* and *hCEL*; Gene expression levels are expressed as fold changes relative to *Gapdh* mRNA levels. (*G*) mRNA expression of *hCEL-HYB1* and *hCEL* relative to mouse *Cel*. Mean ± standard deviation (SD). Significance (exact *P* values as indicated) was determined by 1-way analysis of variance with Sidak's multiple comparisons. Homozygous mice of both *hCEL-HYB1* and *hCEL* were used for Western blot, immunohistochemistry, and quantitative PCR analysis. (*H*) Western blot analysis of CEL protein expression in the pancreas of homozygous (*hCEL-HYB1*+/+) and heterozygous (*hCEL-HYB1*+/−) mice. β-actin was measured as a loading control.

mouse *Cel* gene's upstream sequence, the *hCEL* and *hCEL-HYB1* transcripts in mouse pancreas are present at only 46% of the level of the murine *Cel* transcripts (Figure 2*F*, *G*). Compared with heterozygotes, homozygous *hCEL-HYB1* mice expressed higher levels of hCEL-HYB1 protein (Figure 2*H*). Most of the *CEL-HYB1* alleles are found in the heterozygous state in patients except 1 homozygote in French cohort.[20] However, except for observation of spontaneous pancreatitis, we used homozygous mice in our experiments, which exhibited relatively more obvious and earlier pancreatic lesions.

Pathological Changes Characteristic of Focal Pancreatitis in hCEL-HYB1 Mice

hCEL-HYB1 and *hCEL* mice demonstrated no obvious physical or behavioral changes and bred normally relative to wild-type C57BL/6J littermates. However, although both transgenic mice exhibited normal weight gain up to 1 year of age (Figure 3*A*), pancreas weight analysis demonstrated slight atrophy in the *hCEL-HYB1* mice relative to C57BL/6J and *hCEL* strains (Figure 3*B*). Histological examination of the pancreata isolated from the *hCEL-HYB1* mice revealed focal pancreatic damage (Figure 3*C*). The earliest anomaly noted was mild vacuolization of acinar cells in the pancreas sections of the *hCEL-HYB1* mice. In addition, some *hCEL-HYB1* mice demonstrated focal inflammatory infiltration as well as acinar cell atrophy, and developed a more severe phenotype with increasing age. Compared with homozygotes, the heterozygous *hCEL-HYB1* mice developed similar pancreatic lesions but with less severity and on a slower time-scale (Figure 3*D*). Chronic fibrotic changes were corroborated by Masson's trichrome staining (Figure 3*E*). Infiltration of immune cells was confirmed by immunohistochemistry using the leukocyte common marker Cd45 and the macrophage marker F4/80 (Figure 3*F*, *G*). Quantitative analysis indicated significantly elevated levels of CD45-positive and F4/80-positive cells in *hCEL-HYB1* mice compared with either C57BL/6J or *hCEL* mice (Figure 3*H*, *I*).

Positive staining for cleaved caspase-3 and terminal deoxynucleotidyl transferase dUTP nick end labeling (TUNEL) indicates that apoptosis plays a critical role in the pancreatic injury observed in *hCEL-HYB1* mice (Figure 4*A*, *B*). Quantitative analysis showed the pancreatic sections from *hCEL-HYB1* mice had more numerous TUNEL-positive cells than that from controls at 1 year of age (Figure 4*C*). We also observed that some pancreatic acinar cells of *hCEL-HYB1* mice could not maintain morphological structure and ruptured. Immunohistochemistry showed that Hmgb-1 was translocated from nucleus to cytoplasm in these affected acinar cells, indicating cellular injury (Figure 4*D*). In addition, aged *hCEL-HYB1* mice developed eosinophilic inclusion bodies and increased vacuolization in the acinar cells; immunohistochemistry showed that these eosinophilic bodies were strongly positive for hCEL-HYB1 protein staining (Figure 4*E*). Up to 12 months of age, approximately 15% of *hCEL-HYB1* mice exhibited pathological changes characteristic of pancreatitis, whereas sections from C57BL/6J and *hCEL* mice showed normal histological architecture of the pancreas. However, despite the presence of focal pancreatic lesions, we did not observe the full spectrum of features of progressive fibrotic pancreatitis in the pancreata of *hCEL-HYB1* mice.

Proteotoxic Misfolding and ER Stress in hCEL-HYB1 Mice

To evaluate the secretion, function, and misfolding of the hCEL-HYB1 protein in vivo, pancreatic acini isolated from *hCEL-HYB1* and *hCEL* mice were cultivated in culture medium. The CEL protein content was then measured in intracellular fraction, medium, soluble fraction, and insoluble fraction by Western blotting analysis: the amount of hCEL-HYB1 protein in the conditioned medium of pancreatic acini from *hCEL-HYB1* mice was significantly lower than that of the hCEL protein from *hCEL* mice; essentially all of the hCEL protein was soluble whereas a considerable fraction of the intracellular hCEL-HYB1 protein was present in an insoluble form (Figure 5*A*, *B*). These results indicate that the hCEL-HYB1 protein exhibits defective secretion and tends to accumulate as insoluble aggregates within pancreatic acinar cells.

To determine whether the hCEL-HYB1 protein triggers ER stress and an unfolded protein response (UPR) in mouse pancreas, we measured the expression of ER stress markers in pancreatic tissue homogenate. The expression levels of the ER stress-induced transcription factor sXbp1 (the spliced form of X-box binding protein-1) and the ER stress-related pro-apoptotic transcription factor Ddit3 were significantly increased in *hCEL-HYB1* mice as compared with C57BL/6J and *hCEL* controls (Figure 5*C*, *D*). The ER chaperone protein Hspa5, which is involved in protein folding and quality control in the ER, was slightly increased in total tissue protein and showed significant up-regulation in the insoluble fraction of *hCEL-HYB1* mice (Figure 5*C*, *D*). Elevated expression of Ddit3 and Hspa5 was further confirmed by quantitative reverse transcriptase polymerase chain reaction (qRT-PCR) analysis (Figure 5*E*, *F*). The up-regulation of *Hspa1a*, *Hsp90aa1*, and *Hsp90ab1* mRNAs indicated that hCEL-HYB1 protein induced cellular stress and triggered an adaptive response that could be expected to promote protein folding and to relieve ER stress (Figure 5*G*, *H*, *I*). To test for another possible mechanism, we measured trypsin activity in the pancreata of the 3 mouse strains and found no significant difference in trypsin activity between *hCEL-HYB1* mice and controls (Figure 5*J*).

Autophagy in hCEL-HYB1 Mice

To measure the autophagy level in vivo, we detected LC3 by immunofluorescence on pancreatic sections from mice aged 8 and 24 weeks. Relative to C57BL/6J and *hCEL* samples, more fluorescent dots were observed in the cytoplasm of acinar cells of *hCEL-HYB1* mice at 24 weeks of age (Figure 6*A*). We then analyzed the expression of the autophagy-related proteins LC3, p62, and beclin1. To improve our ability to detect the expression of p62, we used ultra-sensitive enhanced chemiluminescence reagent.
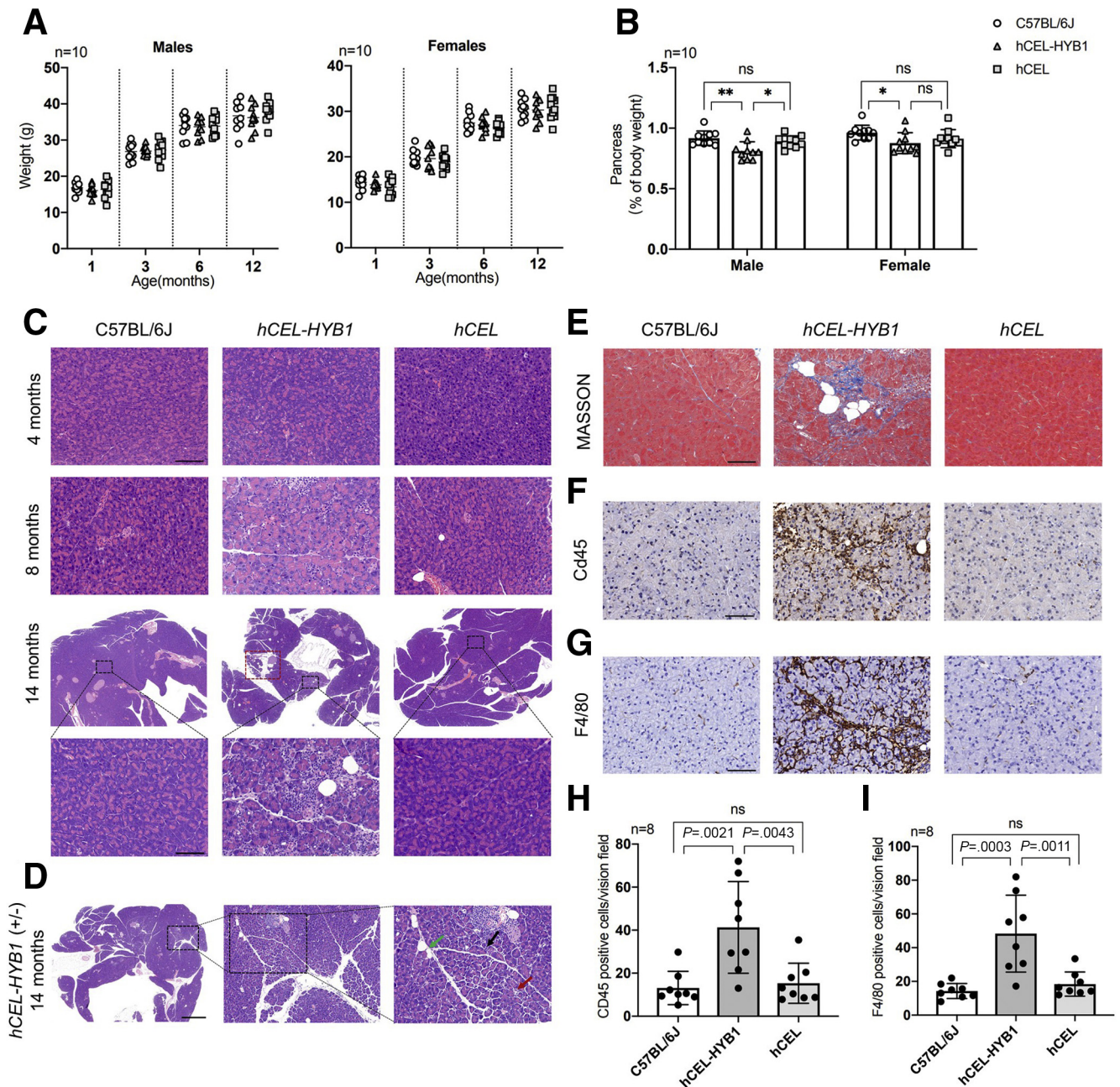
Figure 3. Histological analysis of C57BL/6J, *hCEL-HYB1*, and *hCEL* mice. (*A*) Body weight of each mouse strain at 1 month, 3 months, 6 months, and 12 months of age. (*B*) The relative pancreas weights of each mouse strain, expressed as a percentage of body weight, at 12 months of age. Mean ± standard deviation (SD). *P < .05; **P < .01; 1-way analysis of variance with Sidak's multiple comparisons. (*C*) Representative hematoxylin and eosin (H&E)-stained tissue sections of pancreas isolated from homozygous *hCEL-HYB1*, *hCEL*, or wild-type C57BL/6J mice of different ages. Representative H&E images from 4-month-old *hCEL-HYB1* mice showing mild vacuolization of the acinar cells (*top*). Pancreatic section from an 8-month-old *hCEL-HYB1* mouse showing focal immune cell infiltration and loss of adjacent acinar cells (*middle*). More severe inflammatory infiltration, fibrotic reaction, and fatty changes (*red dotted box*) in pancreatic tissue from a 14-month-old *hCEL-HYB1* mouse (*bottom*). Scale bar = 100 μm. (*D*) Representative H&E-stained tissue section of pancreas isolated from a heterozygous *hCEL-HYB1* mouse at 14 months of age showing inflammatory infiltration (*black arrow*), fatty changes (*green arrow*), and acinar atrophy (*red arrow*). Scale bar = 1 mm. (*E*) Masson's trichrome staining showing fibrotic changes (*blue color*) resulting from the destruction of acini. Scale bar = 100 μm. (*F* and *G*) Immunohistochemistry for Cd45 and F4/80 demonstrates focal areas of immune cell infiltration in the pancreata of *hCEL-HYB1* mice. Scale bar = 100 μm. (*H* and *I*) Quantification under the light microscope of Cd45-positive and F4/80-positive cells for C57BL/6J, *hCEL-HYB1*, and *hCEL* mice aged 12 months. Mean ± SD (n = 8). Significance (exact P values indicated) was determined by 1-way analysis of variance with Sidak's multiple comparisons.
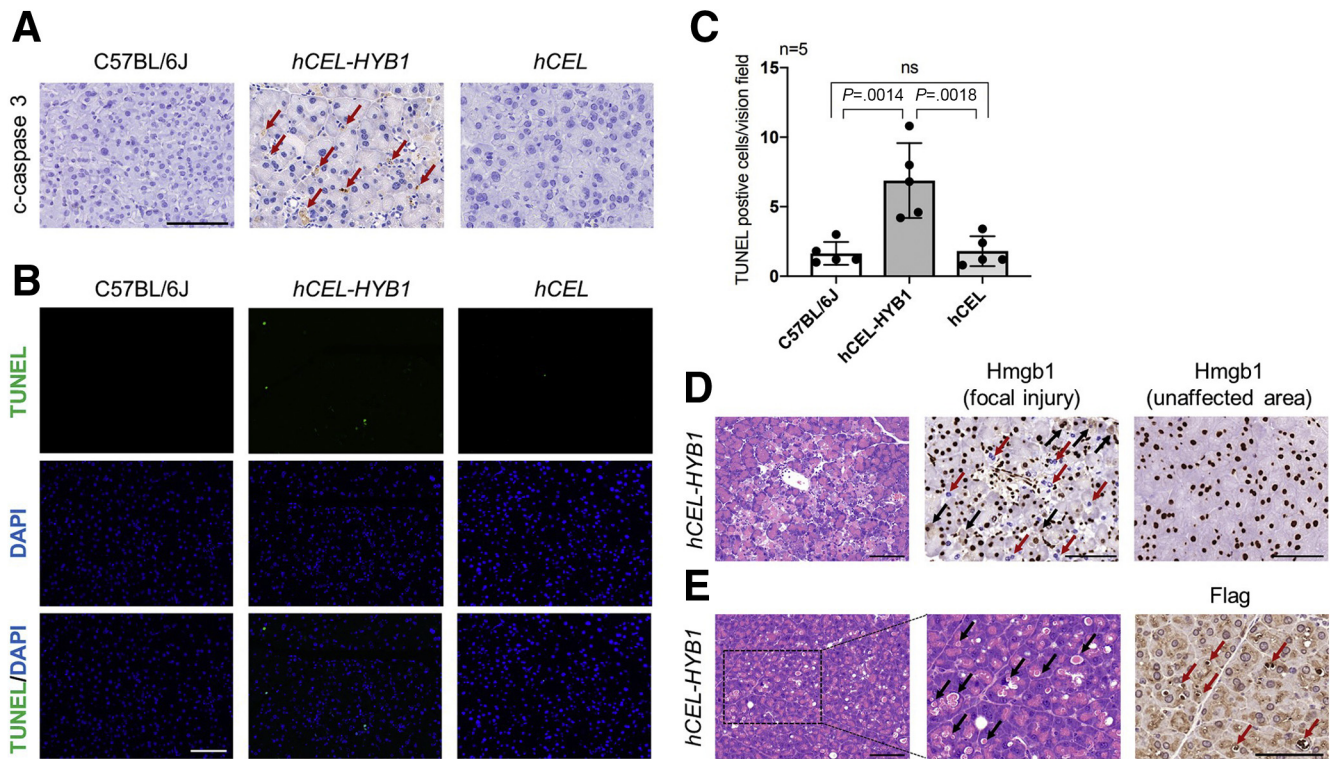
Figure 4. Apoptosis, focal injury, vacuolization, and eosinophilic inclusion bodies of pancreatic acinar cells in *hCEL-HYB1* mice. (*A*) Immunohistochemistry for the apoptosis marker, cleaved caspase-3, as well as (*B*) TUNEL assay, used to detect DNA breaks formed during apoptosis, performed on pancreas sections from C57BL/6J, *hCEL-HYB1* and *hCEL* mice at 10 months of age. *Red arrows* mark representative cleaved caspase-3-positive cells. Scale bar = 100 μm. (*C*) Quantitative analysis of TUNEL-positive cell staining in pancreatic sections showed that 1-year-old *hCEL-HYB1* mice developed higher levels of apoptosis than controls. Mean ± standard deviation (SD). Significance (exact *P* values as indicated) was determined by 1-way analysis of variance with Sidak's multiple comparisons. (*D*) Pancreas from a 10-month-old *hCEL-HYB1* mouse exhibited focal destruction of acinar cells, and immunohistochemical analysis for Hmgb1, a characteristic marker of cellular damage. *Red arrows* mark negative staining of Hmgb1 in the nucleus, and *black arrows* mark positive staining of Hmgb1 in the cytoplasm. Scale bar = 100 μm. (*E*) Vacuolization and eosinophilic inclusion bodies (*black arrows*) of acinar cells in the pancreas of a 12-month-old *hCEL-HYB1* mouse. Immunohistochemistry for hCEL-HYB1 protein with anti-Flag antibody (*right*). Scale bar = 100 μm.

Compared with C57BL/6J and *hCEL* controls, the autophagy level was not significantly different in *hCEL-HYB1* mice at 8 weeks (Figure 6*B*). By contrast, LC3-II upregulation with decreased p62 levels was observed in the pancreata of *hCEL-HYB1* mice at 24 weeks (Figure 6*B*). These results indicate that expression of hCEL-HYB1-induced activation of autophagy occurs in mouse pancreas in a time-dependent manner.

Interestingly, we observed severe vacuolization of pancreatic acinar cells in some aged *hCEL-HYB1* mice, and these accumulated intracellular vacuoles were shown to be patchy LC3-positive autophagic vesicles (Figure 6*C*). Some LC3-positive vesicles contain undegraded hCEL-HYB1 protein (Figure 6*D*). Colocalization of LC3 with Lamp1 further revealed that most of these large vesicles were autolysosomes (Figure 6*E*). Immunoblotting showed significant upregulation of both LC3-II and p62 in the pancreata of aged *hCEL-HYB1* mice with severe pancreatic vacuolization (Figure 6*F*). Higher p62 protein expression was further confirmed by immunohistochemistry (Figure 6*G*). Severely vacuolated acinar cells tend to lose their cell morphology and die. However, early vacuolated acinar cells were deemed to be negative for apoptosis and cellular injury, as evidenced by our failure to stain for cleaved caspase-3 and Hmgb1 (Figure 6*H*, *I*).

Ultrastructural Changes of Acinar Cells in hCEL-HYB1 Mice

To evaluate acinar cell architecture in more detail, we performed transmission electron microscopic analysis of the pancreatic tissues. At 5 months of age, *hCEL-HYB1* mice exhibited well-preserved acinar architecture and comparable numbers and morphology of zymogen granules in acinar cells as compared with controls. We observed slightly dilated endoplasmic reticula and vacuolization in acinar cells from *hCEL-HYB1* mice (Figure 7*A*). Some vacuoles that possessed multi-membranous layers were degradative vacuoles (Figure 7*B*). Notably, pancreatic sections from aged *hCEL-HYB1* mice revealed protein aggregates in the cytoplasm of acinar cells (Figure 7*C*), large autophagy vesicles containing undegraded contents (Figure 7*D*), and pronounced ER dilation in some acinar cells (Figure 7*E*), but not in C57BL/6J and *hCEL* animals.

Expression of hCEL-HYB1 Increased the Severity of Caerulein-induced Pancreatitis

To explore whether the *hCEL-HYB1* mice were more susceptible to experimental acute pancreatitis (AP), we challenged 6-month-old *hCEL-HYB1, hCEL* and C57BL/6J mice with a total of 12 injections of caerulein at a supraphysiological dose (50 μg/kg/h), administered hourly (Figure 8A). Pancreata were collected at 24 hours after the
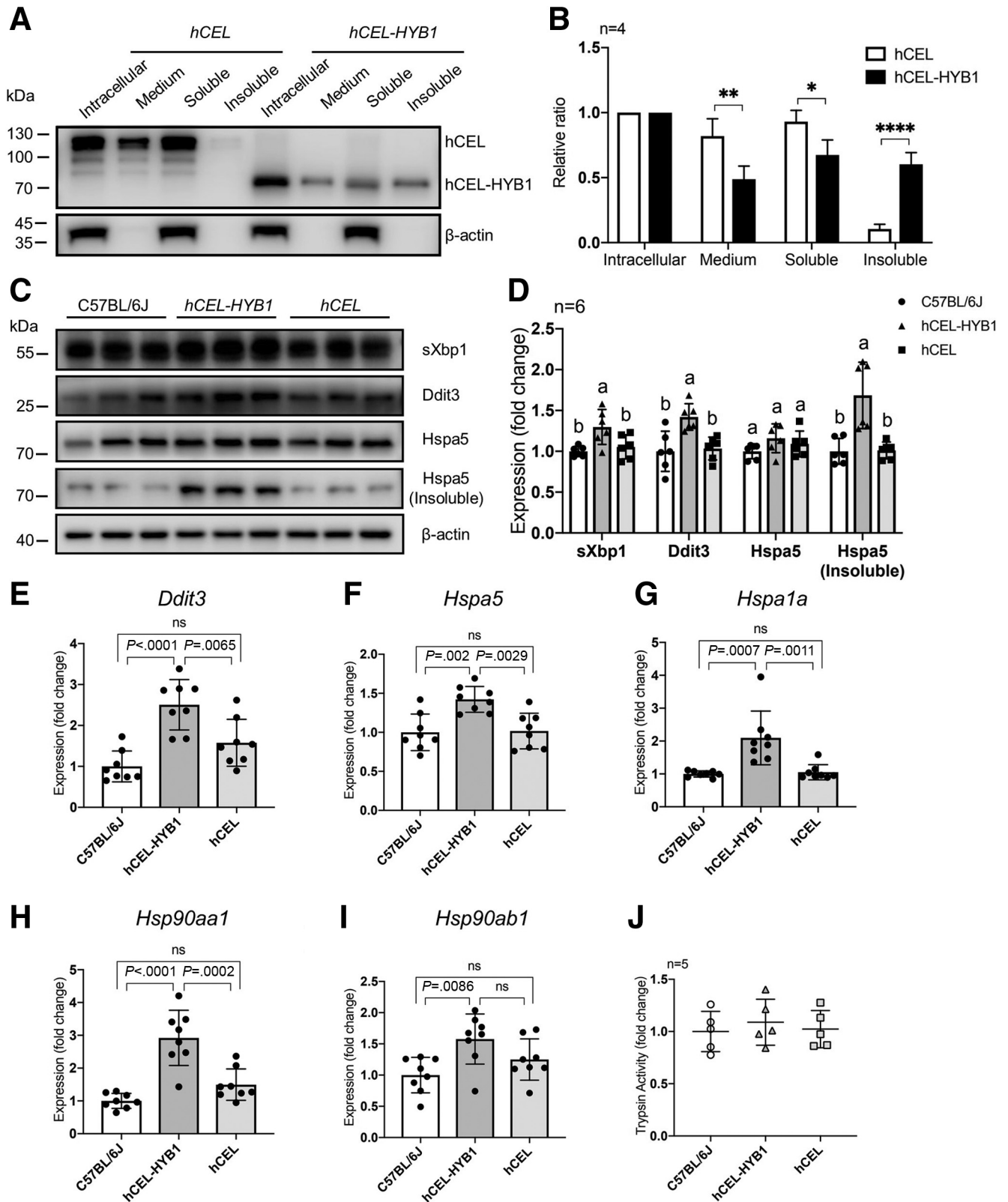
first caerulein injection. *hCEL-HYB1* mice displayed pathological features characteristic of more severe pancreatitis relative to the *hCEL* and C57BL/6J mice (Figure 8B). Pancreata from *hCEL-HYB1* mice exhibited increased cleaved caspase-3-positive cells (Figure 8C). Semi-quantitative analysis of the histological features of pancreatitis demonstrated that the *hCEL-HYB1* mice exhibited more extensive edema and inflammatory infiltration, necrosis and a higher overall histopathological score (Figure 8D). These histological findings were further confirmed by elevated serum amylase activity (Figure 8E). Compared with control mice, *hCEL-HYB1* mice exhibited more significant transcriptional upregulation of ER stress-related markers (Atf4, Hspa5, and Ddit3) under caerulein stimulation (Figure 8F, G, H). In addition, the mRNA levels of pro-inflammatory genes (*Il6* and *Tnf*) and apoptosis-related gene (*Bcl2*) were significantly increased in the *hCEL-HYB1* mice (Figure 8I, J, K).

Next, we assessed whether *hCEL-HYB1* mice would develop more severe CP after a long-term intermittent administration of caerulein (Figure 9A). Compared with *hCEL* and C57BL/6J mice, the *hCEL-HYB1* mice displayed more prominent morphological signs of CP, including acinar cell atrophy, pancreatic duct dilation, immune cell infiltration, and extensive collagen deposition (Figure 9B), which were supported by lower relative pancreas weight and higher histological scores (Figure 9C, D). These histological changes were accompanied by significantly increased levels of the fibrosis marker, Acta2 and the ER stress marker, Hspa5 (Figure 9E, F).

Discussion

The current study investigated for the first time the pathogenic mechanism underlying the *CEL-HYB1* allele in vivo by knocking-in this hybrid allele into the mouse *Cel* locus. Given the sequence differences between the human and mouse *CEL* genes, we generated a human *CEL* knock-in mouse strain (ie, the *hCEL* mice) as an additional control besides the wild-type C57BL/6J mice. Having targeted the *CEL-HYB1* or *CEL* open reading frame into exon 2 of the mouse *Cel* gene, tissue-specific expression of the transgenic gene and silencing of the endogenous *Cel* gene were simultaneously achieved. Notably, in these 2 novel mouse strains, we added a 3×Flag epitope tag at the amino terminus of the CEL or CEL-HYB1. According to the study of Gravdal et al, a V5/His tag on another known pathogenic

variant of CEL (*CEL-MODY*) increased secretion and solubility of CEL-MODY in vitro.[30] However, we failed to observe any significant influence of the 3×Flag epitope tag on the cellular properties of CEL-HYB1 proteins. It should be noted that the *CEL-HYB1* sequence we used to construct the genetic models only contains 1 of the 2 non-synonymous SNPs (c.1463T>C (p. Ile488Thr)) in the breakpoint region of *CEL-HYB1*.[26] *hCEL-HYB1* mice, although not spontaneously developing extensive fibrotic pancreatitis, showed focal pancreatic injury characterized by acinar atrophy, vacuolization, intralobular inflammatory, and focal fibrosis. In contrast to heterozygous state of *CEL-HYB1* allele in most patients, *hCEL-HYB1* mice were bred to homozygosity to obtain stronger and earlier responses, which was more practical for our experimental studies. This strategy was commonly used in the study of pancreatitis-related gene mutations in animal models before.[6,19]

To determine whether the hybrid variant caused protein misfolding in vivo, we investigated protein secretion and markers of ER stress in the *hCEL-HYB1* strain. The hCEL-HYB1 fusion protein displayed reduced secretion and served to induce ER stress in the mouse pancreas, as evidenced by elevated levels of Hspa5, Ddit3, and spliced Xbp1. However, modestly increased levels of *Hspa5* and *Ddit3* mRNA indicated that ER stress was maintained at a relatively low level, which is consistent with the moderate dilation of the ER in acinar cells. The up-regulation of *Hspa1a* and *Hsp90* mRNA and activation of UPR suggests that the expression of hCEL-HYB1 may cause adaptive responses. Compared with young *hCEL-HYB1* mice, aged *hCEL-HYB1* mice exhibited higher levels of acinar cell apoptosis, as a result of the accumulation of misfolded proteins and the prolonged activation of ER stress.

Consistent with previous in vitro studies,[26,31] high levels of hCEL-HYB1 in the detergent-insoluble fraction indicate that the fusion protein tends to aggregate in acinar cells compared with the hCEL protein, a finding that was further confirmed by the formation of hCEL-HYB1-positive eosinophilic inclusion bodies and cytoplasmic protein aggregates observed under the electron microscope. It is worth mentioning that these pathological changes in the mouse pancreas appear to be age-related. Notably, the *CEL-MODY* variant, containing a modified C-terminus caused by single-base deletion, induces ER stress, UPR, and cell apoptosis.[32] The aberrant and truncated carboxy terminal end of *CEL-*

Figure 5. (*See previous page*). **Proteotoxic misfolding and ER stress in *hCEL-HYB1* mice.** (*A*) Protein content of hCEL and hCEL-HYB1 in intracellular fraction, medium, and soluble and insoluble fractions from isolated acinar cells were analyzed by Western blotting using an anti-Flag antibody. Data are representative of 4 independent experiments. (*B*) Estimation of CEL content by densitometry of immunoblots (n = 4). For each subtype, CEL content in the intracellular fraction was arbitrarily set to 1.0. Mean ± standard deviation (SD). *$P < .05$; **$P < .01$; ****$P < .0001$; ns, $P > .05$; 2-tailed unpaired Student *t* test. (*C*) Immunoblots of sXbp1 (soluble), Ddit3 (soluble), Hspa5 (soluble and insoluble) in pancreatic tissue homogenates of *hCEL-HYB1*, *hCEL*, and C57BL/6J mice aged 5 months. (*D*) Quantification of bands after adjustment to the β-actin levels. Mean ± SD (n = 6). Bars with different letters represent significant differences in means by 1-way analysis of variance with Sidak's multiple comparisons. (*E-I*) Messenger RNA expression of *Ddit3*, *Hspa5*, *Hspa1a*, *Hsp90aa1*, and *Hsp90ab1* was measured by quantitative PCR. Results were expressed as fold change relative to the C57BL/6J results. Mean ± SD (n = 8). Significance (exact *P* values indicated) was determined by 1-way analysis of variance with Sidak's multiple comparisons. (*J*) Pancreatic trypsin activity in C57BL/6J, *hCEL-HYB1*, and *hCEL* mice at 5 months of age showing no significant difference. Data shown are mean ± SD; 1-way analysis of variance test.
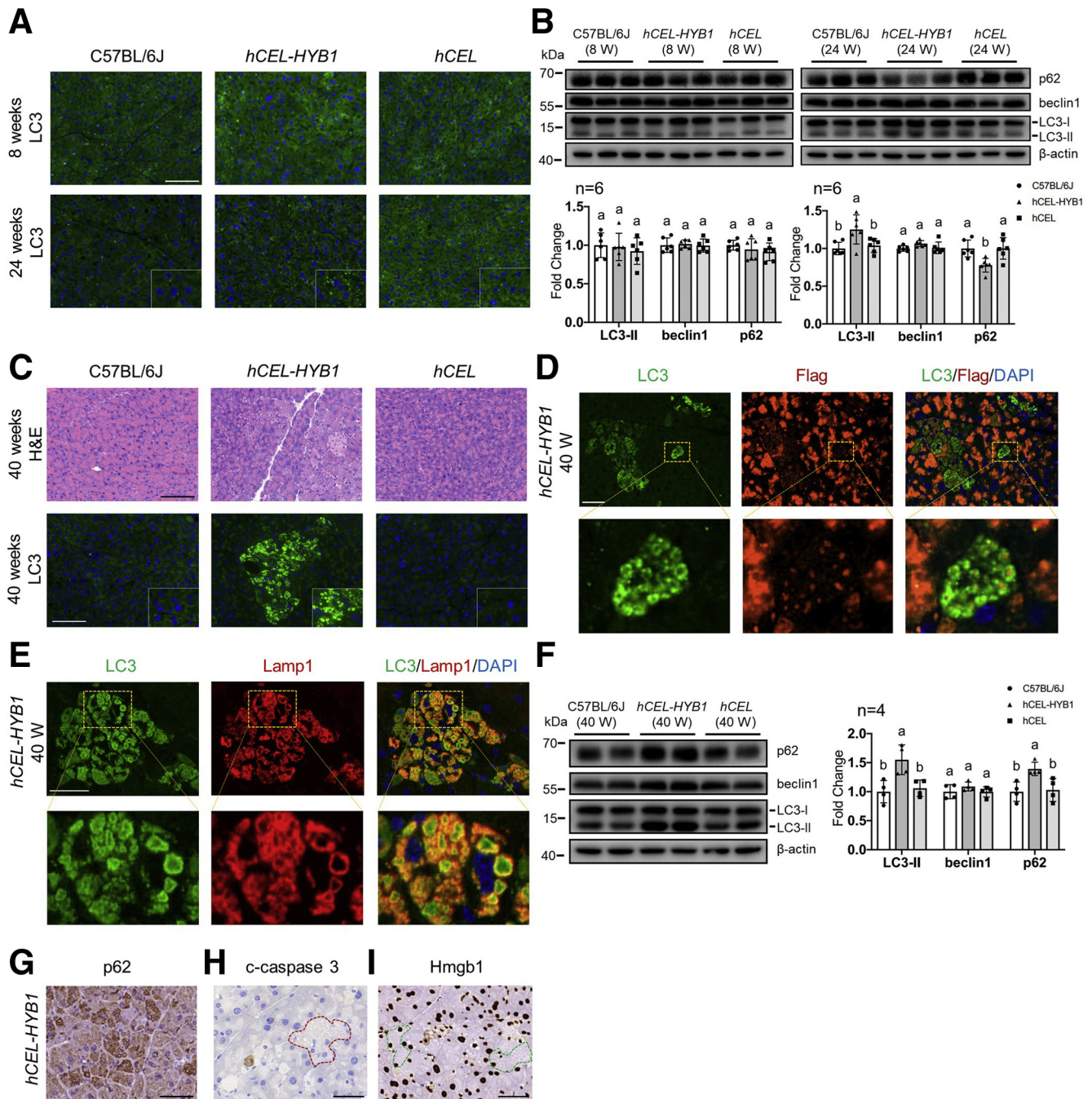
Figure 6. Autophagy in *hCEL-HYB1* mice. (*A*) Representative anti-LC3 immunofluorescence staining in pancreatic sections from mice aged 8 weeks and 24 weeks. The images display LC3 signals in *green*, and cell nuclei in *blue*. Scale bar = 100 μm. (*B*) Expression levels of p62, beclin1, and LC3 in pancreatic homogenates from C57BL/6J*, hCEL-HYB1*, and *hCEL* mice aged 8 weeks and 24 weeks were detected by Western blot (*upper panel*). Bottom, quantification of bands after adjustment to the β-actin. Mean $\pm$ standard deviation (SD) (n = 6). Bars with different letters represent significant differences in means by 1-way analysis of variance with Sidak's multiple comparisons. (*C*) Pancreatic section from a 40-week-old *hCEL-HYB1* mouse showing cytoplasmic vacuolization of acinar cells (*upper*). LC3 immunofluorescence staining in pancreatic sections with severely vacuolated acinar cells (*down*). Scale bar = 100 μm. (*D* and *E*) Co-localization of LC3-positive vacuoles with hCEL-HYB1 (Flag) or Lamp1 in pancreatic sections from a 40-week-old *hCEL-HYB1* mouse with severe vacuolation of acinar cells. Scale bar = 40 μm. (*F*) Expression levels of p62, beclin1, and LC3 in pancreatic homogenates from *hCEL-HYB1* mice with severe cytoplasmic vacuolation of acinar cells were detected by Western blot analysis (*left panel*). Right, quantification of bands after adjustment to the β-actin. Mean $\pm$ SD (n = 4). Bars with different letters represent significant differences in means by 1-way analysis of variance with Sidak's multiple comparisons. (*G-I*) Immunohistochemical analysis for p62, cleaved caspase-3, and Hmgb1 in early vacuolated acinar cells. *Red dotted line* outlines the area of severely vacuolated acinar cells showing negative cleaved caspase-3 staining (*middle*). *Green dotted line* outlines the vacuolated acinar cells without obvious nuclear-cytoplasmic translocation of Hmgb1 (*right*). Scale bar = 40 μm.
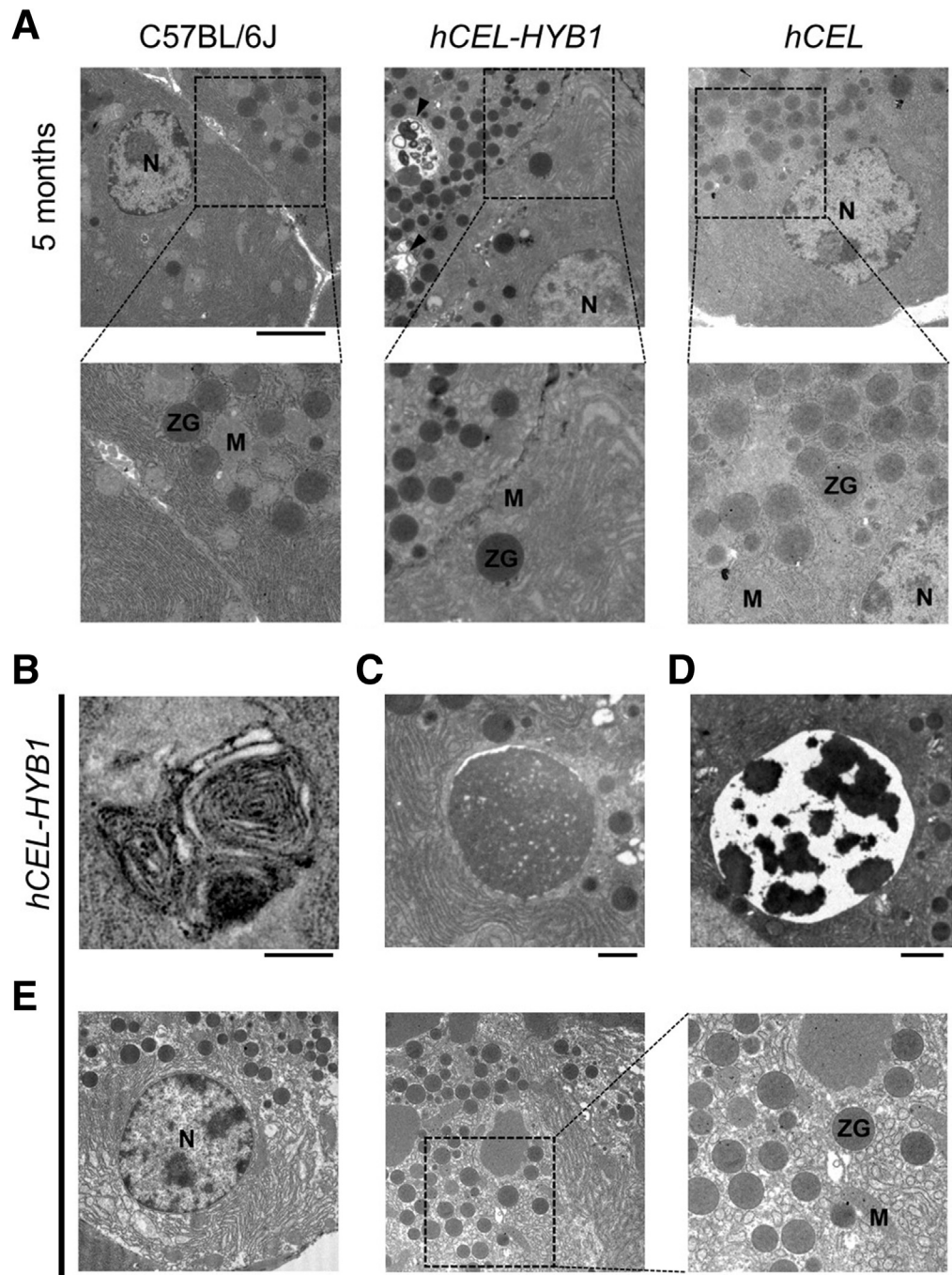
Figure 7. Ultrastructural changes in *hCEL-HYB1* mice. (*A*) Representative transmission electron micrographs of pancreas from C57BL/6J, *hCEL-HYB1*, and *hCEL* mice aged 5 months. *hCEL-HYB1* mice show slightly dilated endoplasmic reticula and vacuolation (*black arrow*). Scale bar = 4 μm. (*B*) Degradative vacuoles in an acinar cell from an *hCEL-HYB1* mouse aged 6 months. Scale bar = 0.5 μm. Pancreatic tissue sections from 12-month-old *hCEL-HYB1* mice showing protein aggregates in cytoplasm (Scale bar = 1 μm) (*C*); large autophagy vesicles with undegraded high-density contents (Scale bar = 2 μm) (*D*); as well as evident dilated endoplasmic reticula in some acinar cells (Scale bar = 4 μm) (*E*).

HYB1 derived from *CELP* may be responsible for the increased formation of intracellular aggregates relative to hCEL.[26] In addition, misfolded proteins that escape degradation may be prone to aggregation, because they often expose hydrophobic surfaces leading to abnormal protein-protein interactions.[33] The elevated levels of apoptosis in the pancreas of aged *hCEL-HYB1* mice could be associated with prolonged ER stress, as well as secondary injury caused by cellular endocytosis of extracellular hCEL-HYB1 protein.[27]

We next investigated autophagic activity in the pancreas from *hCEL-HYB1* mice of different age groups. Compared with control strains, autophagy was activated in 24-week-old *hCEL-HYB1* mice, but not in 8-week-old *hCEL-HYB1* mice. Autophagy plays an important role in maintaining pancreatic acinar cell homeostasis, and autophagic dysfunction can lead to pancreatitis.[34,35] Thus, gradual accumulation of hCEL-HYB1 might induce the autophagic elimination of defective protein to maintain cellular homeostasis. Notably, we observed the significant accumulation of large

autophagic vesicles in the acinar cells of some aged *hCEL-HYB1* mice as well as up-regulated expression of p62 and LC3-II, suggesting that long-term exposure to hCEL-HYB1 might induce autophagy deficiency in pancreatic acinar cells.

Protein homeostasis in cells is maintained through a delicate balance between protein synthesis, folding, and degradation. If this equilibrium is disturbed, surplus or misfolded proteins start to accumulate and may inhibit
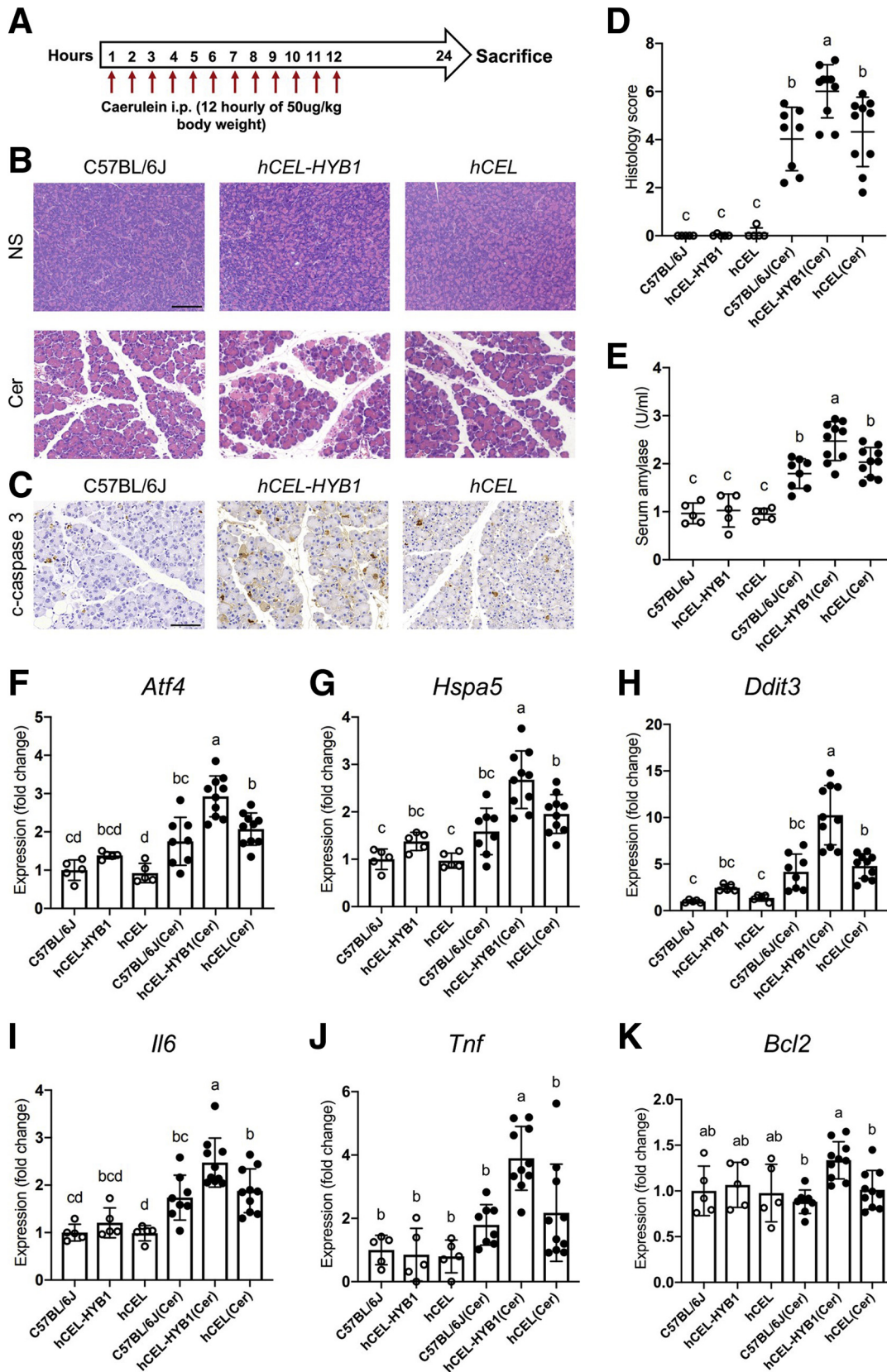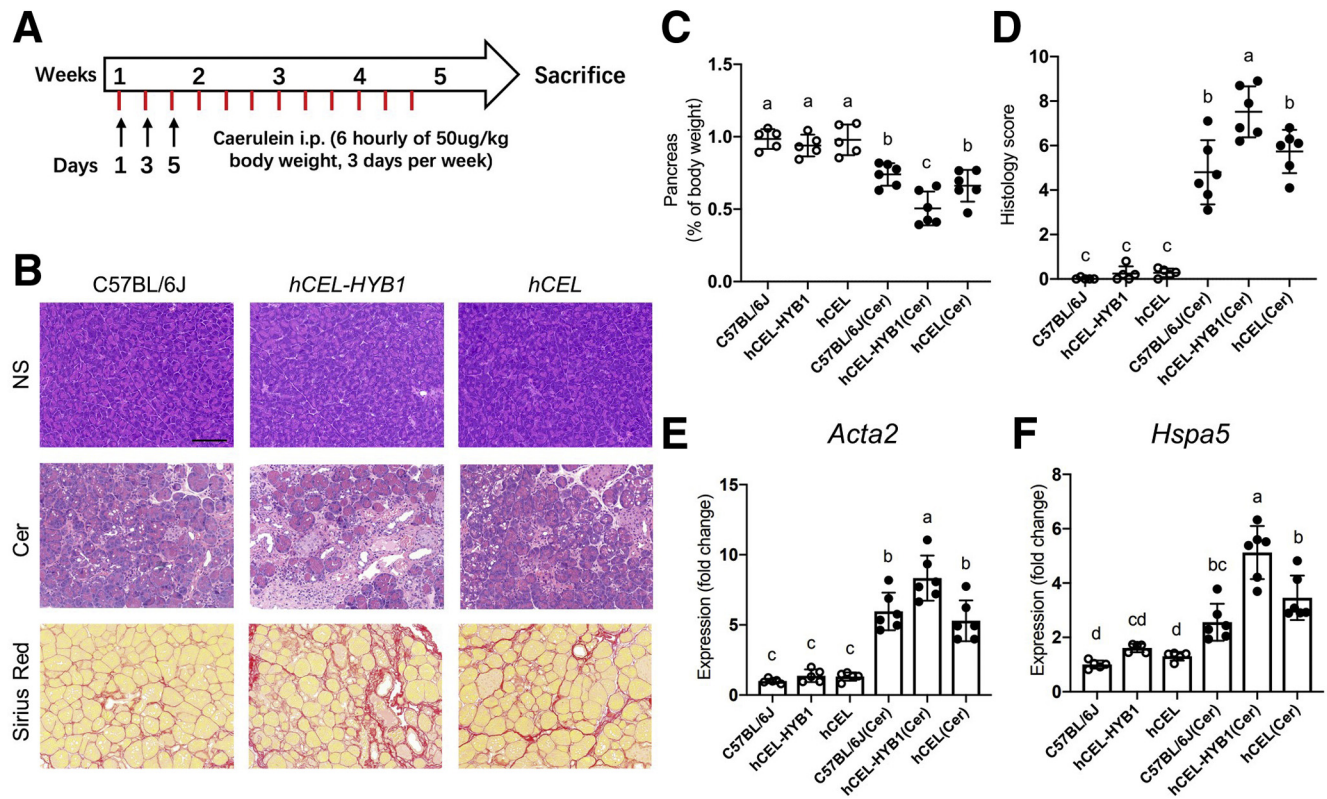
Figure 9. Caerulein-induced chronic pancreatitis in C57BL/6J, *hCEL-HYB1*, and *hCEL* mice. (*A*) Flow diagram of caerulein-induced CP: 6 daily caerulein injections (50 ug/kg body weight), given 1 hour apart, on days 1, 3, and 5 of each week, for 4 weeks. (*B*) Representative images of hematoxylin and eosin (H&E)- and Sirius red-stained tissue sections isolated from C57BL/6J, *hCEL-HYB1*, and *hCEL* mice. Scale bar = 100 μm. (*C*) Relative pancreas weights (shown as a percentage of body weight). (*D*) Histologic score and quantitative analysis. (*E-F*) Messenger RNA expression of *Acta2* and *Hspa5* was measured by quantitative PCR. Throughout the Figure, data are presented as mean values ± standard deviation (SD); bars with different letters represent significant differences in means by 1-way analysis of variance with Sidak's multiple comparisons. NS, normal saline; Cer, caerulein.

cellular functions. Because pancreatic acinar cells possess high rates of protein synthesis, correct protein folding and the endogenous clearance of faulty proteins are essential for cellular homeostasis. In the present study, although these 2 humanized mouse strains were constructed using similar genetic strategies and exhibited similar transcript expression levels, the expression level of the hCEL-HYB1 protein in pancreatic tissues was significantly decreased relative to hCEL. The activation of the UPR and autophagy suggests potential routes for degradation of the hCEL-HYB1 protein in acinar cells in the early stage.

Clinically, despite the *CEL-HYB1* variant serving as a risk factor for CP, the majority of *CEL-HYB1* carriers are likely to stay healthy in the general population.[36] The recent report of 2 *CEL-HYB1*-positive families suggests that this hybrid allele promotes the development of CP in combination with other risk factors.[31] When treated with caerulein at a supramaximal dose, *hCEL-HYB1* mice developed more severe AP or CP than controls. Significantly elevated ER stress markers and higher apoptosis levels suggest a synergistic response between *CEL-HYB1* and caerulein hyperstimulation. In addition, pancreatic damage is more likely to occur in elderly *hCEL-HYB1* mice (>8 months). The decreased efficiency of acinar cells in eliminating misfolded proteins may partially account for the age-related AP/CP phenotype in *hCEL-HYB1* mice.

Figure 8. (*See previous page*). **Caerulein-induced acute pancreatitis in C57BL/6J, *hCEL-HYB1*, and *hCEL* mice.** (*A*) For induction of AP, *hCEL-HYB1* and control mice aged 6 months old were given 12-hourly injections of caerulein (50 μg/kg/h). (*B*) Representative images of hematoxylin and eosin (H&E)-stained tissue sections isolated from C57BL/6J, *hCEL-HYB1*, and *hCEL* mice. Scale bar = 100 μm. (*C*) Immunohistochemical analysis for apoptotic cells with anti-cleaved caspase-3 antibody. Scale bar = 100 μm. (*D*) Semi-quantitative histology score examination of H&E-stained sections from 3 mouse strains. (*E*) Serum amylase activity. (*F-H*) Messenger RNA expression of ER stress markers Atf4, Hspa5, and Ddit3 was measured by quantitative PCR. (*I-K*) Messenger RNA expression of *Il6*, *Tnf*, and *Bcl2*. Throughout the Figure, data are presented as mean values ± standard deviation (SD); bars with different letters represent significant differences in means by 1-way analysis of variance with Sidak's multiple comparisons. NS, normal saline; Cer, caerulein.

The *CPA1* N256K mouse strain was the first enzyme misfolding-associated animal model of CP, which served to introduce the human pathogenic point mutation into the mouse *Cpa1* locus. By contrast, the *CEL-HYB1* variant is caused by exchange of large DNA fragment between *CEL* and *CELP*. Compared with the spontaneous and progressive pancreatic damage in *CPA1* N256K mice, *hCEL-HYB1* mice demonstrated relatively minor and localized pancreatic lesions with lower disease penetrance, consistent with the moderate upregulation of the pro-apoptotic transcription factor, Ddit3. There are several potential explanations for the differences. First, *CPA1* variants that elicit misfolding have a strong, essentially disease-causing impact, whereas the *CEL-HYB1* variant only serves as a moderate risk factor for CP. Second, in spite of the hCEL-HYB1 protein showing impaired secretion in this study, part of this enzyme can still be transported out of the pancreatic acinar cells. Third, a relatively low level of hCEL-HYB1 mRNA and protein in acinar cells could limit its proteotoxicity. Fourth, the relative weak pancreatic phenotype may be caused by species-specific differences, as rodent *Cel* genes have a markedly shorter C-terminal VNTR than their human *CEL* counterpart.[37]

In conclusion, we provide cogent evidence to support our contention that the *CEL-HYB1* hybrid allele induces protein misfolding and promotes pancreatitis in a mouse model. Adaptive responses, such as UPR and autophagy, may serve both to control and limit the amount of toxic misfolded proteins generated and to restore protein homeostasis to a certain extent. However, accumulation of misfolded proteins and prolonged endoplasmic reticulum stress could eventually lead to pancreatic damage. An improved understanding of protein homeostasis and the mechanisms of endogenous clearance of misfolded proteins in pancreatic acinar cells may facilitate the development of novel therapeutic strategies for CP.

Methods

CEL Variant Plasmid Constructions and Transfection

cDNA encoding full length wild-type CEL, 3×Flag-tagged wild type CEL, CEL-HYB1, or 3×Flag-tagged CEL-HYB1 was cloned into the pcDNA3.1 vector. All final DNA constructs were confirmed by DNA sequencing. For transfection of HEK293T cells, Lipofectamine 2000 was used according to the manufacturer's instructions. Cells were transfected with plasmids encoding wild-type CEL or CEL-HYB1, either with or without the 3×Flag tag. Cells transfected with empty vector were included as a negative control.

Cell Fractionation and Collection of Conditioned Media

Forty-eight hours post-transfection, conditioned medium was harvested and analyzed as the medium fraction. Cells were rinsed twice with ice-cold phosphate-buffered saline (PBS), and lysed with radio-immunoprecipitation assay (RIPA) buffer (P0013B, Beyotime) supplemented with protease inhibitor cocktail (ab201119, Abcam). After 30

minutes incubation on ice, the lysate was centrifuged at 16,000g for 15 minutes at 4 °C. The supernatant was isolated and analyzed as the soluble lysate fraction. Protein concentration was measured using a bicinchoninic acid (BCA) assay (Thermo Fisher Scientific). The pellet was washed twice in ice-cold PBS and re-suspended in 60 μl sample buffer. The resuspensions were sonicated until no visible particles remained. The resulting resuspensions were analyzed as the insoluble pellet fraction. The soluble lysates of 10 μg total protein were examined by Western blotting. For the medium and pellet fractions, the volume loaded onto the sodium dodecyl sulfate-polyacrylamide gel was the same as for the corresponding soluble lysate.

Generation of Humanized CEL-HYB1 and CEL Mouse Strains

All mice used in this study were on a C57BL/6J genetic background. The humanized *CEL-HYB1* and *CEL* mouse strains (termed *hCEL-HYB1* and *hCEL* mice, respectively) were generated by Shanghai Model Organisms (Shanghai, China) using CRISPR/Cas9-mediated genome engineering. The mouse *Cel* gene, located on chromosome 2, contains 11 exons. The targeting vector contained the *hCEL-HYB1* exon2∼11-3×Flag-*mCel* 3′UTR-sv40 polyA or the *hCEL* exon2∼11-3×Flag-*mCel* 3′UTR-sv40 polyA frame (Figure 10*A*, *B*). Cas9 mRNA, gRNA, and targeting vector were injected into the cytoplasm of fertilized eggs collected from C57BL/6J mice, which were implanted into pseudo-pregnant females. Positive F0 mice were identified by long-range polymerase chain reaction (PCR) followed by Southern blot verification and sequencing. The F0 generation mice were backcrossed to C57BL/6J mice to obtain heterozygous F1 mice, which were further verified by PCR amplification and sequencing. For experimental analyses, sex- and age-matched animals were sacrificed at specified times. Both male and female animals were studied. All mouse strains were housed in a specific pathogen-free barrier facility at Shanghai Model Organisms and were housed in a humidity- and temperature-controlled room with a 12-hour light/dark cycle. All animal studies were performed in compliance with the ethical guidelines for animal studies and approved by the Institutional Animal Care and Use Committee of the Second Military Medical University.

Genotyping

Mice tails (0.2cm) were snipped at 3 weeks of age. DNA was extracted from tail snips using DNeasy Blood and Tissue kit according to the manufacturer's instructions (Qiagen). We designed specific primers to identify the respective genotypes by PCR (for details, see Figure 10*C*, *D*).

Histology and Immunohistochemistry

Most of the pancreatic tissue from each mouse (except a small piece of tissue for PCR or immunblot analysis) was removed and fixed in 10% neutral buffered formalin overnight. Then, tissues were embedded in paraffin, and 5-μm sections were taken and mounted on slides for staining.

Subsequently, tissue sections were stained with hematoxylin and eosin staining for histopathological evaluation. Masson's trichrome staining (ab150686, Abcam) was performed according to the manufacturer's instructions. Immunohistochemical staining was performed on paraffin sections using antibodies against CEL (15384-1-AP, Proteintech, China), Flag (AT0022, CMCTAG), cleaved caspase-3 (#9664, Cell Signaling Technology), HMGB1 (ab79823, Abcam), F4/80 (#70076, Cell Signaling Technology), CD45 (ab10558, Abcam), and P62 (18420-1-AP, Proteintech). After deparaffinization and rehydration, antigen retrieval was performed by boiling slides in citrate buffer (10 mM citric acid, pH 6.0) for 15 minutes. Endogenous peroxidase activity was blocked with 3% hydrogen peroxide for 15 minutes at room temperature in the dark. Tissue sections were incubated with the primary antibody diluted in blocking solution overnight at 4 °C. Appropriate secondary antibodies were applied for 1 hour at room temperature. Staining was then developed by incubating with diaminobenzidine. CD45-positive cells and F4/80-positive cells were quantified as the average number per visual field (40× magnification) from at least 5 randomly selected fields per section. For immunofluorescence staining, paraffin-embedded pancreas biopsy sections were stained with antibodies against LC3 (#12741, Cell Signaling Technology), Flag (AT0022, CMCTAG) and LAMP1 (#9091, Cell Signaling Technology), and secondary fluorescent antibody (SA00013-2/SA00013-3/SA00013-4, Proteintech). The TUNEL staining was carried out using a TUNEL staining kit according to the manufacturer's instructions (Roche). For quantification of TUNEL-positive cells, tissue sections were analyzed at 40× magnification, and TUNEL-positive cells were counted.

Trypsin Activity Assay

Trypsin activity was assessed using the trypsin activity colorimetric assay kit (MAK290, Sigma) according to the manufacturer's instructions. Briefly, small pieces of tissue (∼50 mg) were homogenized in 300 μL trypsin assay buffer and centrifuged at 12,000g at 4 °C for 10 minutes. Total protein concentration of the supernatant was measured by BCA analysis and balanced with trypsin assay buffer, which was then used for the trypsin activity test.

Isolation of Pancreatic Acini and Collection of Culture Media and Intracellular Fractions

Pancreatic acini from 6-month-old mice were isolated by collagenase digestion according to the method described by Hegyi et al.[19] Briefly, 30 mg collagenase (LS004188, Worthington) was dissolved into 15 mL incubation buffer (DMEM/F-12 (11039-021, Gibco) supplemented with 1 mg/mL bovine serum albumin (A7030, Sigma), 0.5 mM CaCl2, 2% sodium pyruvate (11360-070, Invitrogen) and 0.1 mg/mL soybean trypsin inhibitor (T9003, Sigma). The pancreas from each mouse was injected with 1.5 mL of the above collagenase digestion solution until well distended. After transfer to a 2-mL centrifuge tube with digestion solution, and incubation in a constant temperature shaker bath (90

rpm for 20 minutes at 37 °C), the pancreas tissue was placed in a 15-mL centrifuge tube with 8 mL incubation buffer and disrupted by pipetting. Subsequently, the cell suspension was filtered through a 100-μm pore-sized nylon mesh. The above steps were repeated until 20 mL cell suspension was obtained from each bulk sample. Cell suspension was centrifuged at 1000 rpm for 1 minute. The supernatant was removed, and the pellet resuspended in 20 mL HEPES solution and incubated at 37 °C for 30 minutes. Acini were resuspended in 5 mL Opti-MEM and then transferred to 6-well tissue culture plates (2 mL into each well). After incubation for 90 minutes at 37 °C, the cell-free media were collected and measured for CEL secretion. The pelleted cells were then washed with PBS solution 3 times and lysed in RIPA buffer (P0013B, Beyotime) containing protease inhibitor mixture (Roche) to obtain intracellular fractions (whole cell lysates). The whole cell lysates were centrifuged at 16,000g for 15 minutes at 4 °C and further processed into detergent soluble and insoluble fractions. The supernatant was isolated and designated as soluble lysate fraction. The final pellets were resuspended in 100 μL sample buffer and sonicated until no particle was visible. This part was analyzed as insoluble fraction. For the intracellular and soluble fractions, equal amounts of lysates containing 15 μg total protein were subjected to immunoblotting. For the medium and insoluble fractions, the volume loaded on the sodium dodecyl sulfate-polyacrylamide gel was normalized on the basis of total protein and β-actin intensity.

Induction of Pancreatitis

For induction of AP, 6-month-old homozygous *hCEL-HYB1*, *hCEL* or wild-type C57BL/6J mice ($\geq$8 animals per group) were starved for 12 hours with free access to water and were then challenged with a total of 12 intraperitoneal injections of caerulein (50 μg/kg/h) administered hourly. The biochemical and pathological parameters of AP were assessed 24 hours after the first injection. Serum was obtained from mice immediately after sacrifice. Serum amylase activity was quantified by amylase assays. To induce CP, 6 intraperitoneal injections of caerulein (50 μg/kg/h) were administered to 5-month-old mice hourly (6 animals per group), 3 days per week, for a total of 4 weeks. The severity of AP or CP was graded by 2 pathologists scoring in double-blind fashion, as previously described.[38,39] The Picro Sirius Red Stain Kit (ab150681, Abcam) was used to evaluate fibrotic collagen deposition according to the manufacturer's instructions. The formula (Pancreata weight/body weight × 100%) was employed to determine the level of pancreatic atrophy in CP.

Western Blot Analysis

Pancreatic tissue (∼30 mg) was homogenized in RIPA lysis buffer (Beyotime Biotechnology) mixed with a protease and phosphatase inhibitor cocktail (ab201119, Abcam). Total protein was purified by centrifugation, and the concentration was determined by means of the BCA kit. An aliquot of the supernatant containing 30 to 60 μg total

A Recombined *hCEL* targeting sequence

......agaaggccgcctagaggcagacactcaccATGGGGCGCCTGGAGGTTCTATTTCTTGGCCTCACCTGCTGCTTGGCAGCGGCTTGTGCTGCAAAGgtaag
ccggaaccctacaagggactacagccctctctcattcactaagatctgggaactggga...cactctggattcaggctagccatgcagaagcccatctgacctg
ccctgtctcacctacagTTGGGGGCTGTGTACACAGAAGGCGGTTTCGTGGAGGGCGTCAACAAGAAGCTCGGCCTCCTGGGTGACTCTGTGGACATCTTCA
AGGGCATCCCCTTCGCAGCTCCCACCAAGGCCCTGGAAAATCCTCAGCCACATCCTGGCTGGCAAGGGACCCTGAAGGCCAAGAACTT...GCTCCATGAAGCG
GAGCCTGAGAACCAACTTCCTGCGCTACTGGACCCTCACCTATCTGGCGCTGCCCACAGTGACCGACCAGGAGGCCACCCCTGTGCCCCCCACAGGGGACTC
CGAGGCCACTCCCGTGCCCCCCACGGGTGACTCCGAGACCGCCCCCGTGCCGCCCACGGGTGACTCCGGGGCCCCCCCCGTGCCGCCCACGGGTGACTCCGG
GGCCCCCCCCGTGCCGCCCACGGGTGACTCCGGGGCCCCCCCCGTGCCGCCCACGGGTGACTCCGGGGCCCCCCCCGTGCCGCCCACGGGTGACTCCGGGGC
CCCCCCCGTGCCGCCCACGGGTGACTCCGGGGCCCCCCCCGTGCCGCCCACGGGTGACTCCGGGGCCCCCCCCGTGCCGCCCACGGGTGACTCCGGCGCCCC
CCCCGTGCCGCCCACGGGTGACGCCGGGCCCCCCCCCGTGCCGCCCACGGGTGACTCCGGCGCCCCCCCCGTGCCGCCCACGGGTGACTCCGGGGCCCCCCC
CGTGACCCCCACGGGTGACTCCGAGACCGCCCCGTGCCGCCCACGGGTGACTCCGGGGCCCCCCCTGTGCCCCCCACGGGTGACTCTGAGGCTGCCCCTGT
GCCCCCCACAGATGACTCCAAGGAAGCTCAGATGCCTGCAGTCATTAGGTTTGACTACAAAGACCATGACGGTGATTATAAAGATCATGATATCGATTACAA
GGATGACGATGACAAGtgaAGTCTTATAAGCTGGGGCTGGAGAGATGGGTCAGGAATTAAGATCACTCA...CCACACAACATACGAGCCGGAAGCATAAAGTG
TAAAGCCTGACTGCCTTTAGCTCTGGTTCTCAAGTCTCTTGGGTGGTGACTCTGTTGACATCTTCAAGGGCATCCCCTTTGCCACTGCCAAGACCTTGGAGA
ATCCTCAGCGTCACCCTGGCTGGCAAGgtgggtgctgagtgctgggtgctgggtgctgggtgctgggtgatgggctggccctggctggttctctttacacct
tgcccttctctcactgtagGGACGCTGAAGGCTACAAACTTCAAGAAACGATGCCTACAGGCCACCATCACCCAGGACAACACCTATGGGCAAGAAGACTGC
CTCTACCTCAATATCTGGGTGCCCCAGGGCAGGAAGCAGGgtatggatcccagtt......

B Recombined *hCEL-HYB1* targeting sequence

......agaaggccgcctagaggcagacactcaccATGGGGCGCCTGGAGGTTCTATTTCTTGGCCTCACCTGCTGCTTGGCAGCGGCTTGTGCTGCAAAGgtaag
ccggaaccctacaagggactacagccctctctcattcactaagatctgggaactggga...cactctggattcaggctagccatgcagaagcccatctgacctg
ccctgtctcacctacagTTGGGGGCTGTGTACACAGAAGGCGGTTTCGTGGAGGGCGTCAACAAGAAGCTCGGCCTCCTGGGTGACTCTGTGGACATCTTCA
AGGGCATCCCCTTCGCAGCTCCCACCAAGGCCCTGGAAAATCCTCAGCCACATCCTGGCTGGCAAGGGACCCTGAAGGCCAAGAACTT...GCTCCATGAAGCG
GAGCCTGAGAACCAACTTCCTGCGCTACTGGACCCTCACCTATCTGGCGCTGCCCACAGTGACCGACCAGGAGGCCAGTTCCATGCCCTCCACAGGGGACTC
TGAGGCCACTCCCGTCTCCCCCGACAGGCAACTCCGAGTCTGCCCCCGTCCCTGCAACGGGGACTACAAAGACCATGACGGTGATTATAAAGATCATGATAT
CGATTACAAGGATGACGATGACAAGtgaAGTCTTATAAGCTGGGGCTGGAGAGATGGGTCAGGAATTAAGATCACTCA...CCACACAACATACGAGCCGGAAG
CATAAAGTGTAAAGCCTGACTGCCTTTAGCTCTGGTTCTCAAGTCTCTTGGGTGGTGACTCTGTTGACATCTTCAAGGGCATCCCCTTTGCCACTGCCAAGA
CCTTGGAGAATCCTCAGCGTCACCCTGGCTGGCAAGgtgggtgctgagtgctgggtgctgggtgctgggtgctgggtgatgggctggccctggctggttctc
tttacaccttgcccttctctcactgtagGGACGCTGAAGGCTACAAACTTCAAGAAACGATGCCTACAGGCCACCATCACCCAGGACAACACCTATGGGCAA
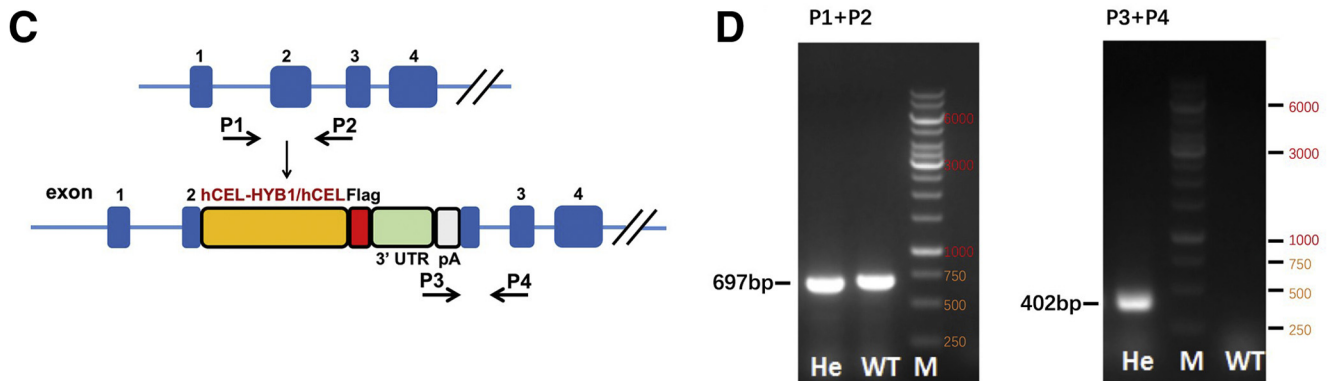GAAGACTGCCTCTACCTCAATATCTGGGTGCCCCAGGGCAGGAAGCAGGgtatggatcccagtt......

C

D

Figure 10. Recombined *hCEL/hCEL-HYB1* targeting sequence and genotyping of mouse strains. (*A* and *B*) The 5′ homology arm and the 3′ homology arm are underlined. The exons of mouse *Cel* are highlighted in green. The 5′ homology arm contains exon 1 plus the proximal portion of exon 2 of mouse *Cel* (including the intervening intron). The 3′ homology arm contains the remainder of exon 2 plus exons 3–7 of mouse *Cel* (including the introns). *hCEL/hCEL-HYB1* exons 2–11 are marked in *yellow*, the VNTR sequences are indicated in *italics*, the 3×Flag is in *red*, and the 3′UTR-polyA is in *blue*. (*C*) Primer design for detecting wild-type and novel knock-in strains. Primers used to genotype mouse *Cel*: 5′-gcggtgggaaagtgcggg-gatagt-3′ (P1) and 5′-cttgccagccagggtgacg-3′ (P2). Primers used to genotype *hCEL-HYB1* or *hCEL*: 5′-gctagagcttggcgtaat-cat-3′ (P3) and 5′-cagtcttcttgcccataggtgt-3′ (P4). (*D*) A representative agarose gel image of the genotyping. The mouse *Cel* amplicon size was 697 bp, whereas both *hCEL-HYB1* and *hCEL* yielded 402 bp PCR products.

protein were subjected to standard Western blotting procedures. Immunoblotting analysis was performed with antibodies against CEL (15384-1-AP, Proteintech), Flag (AT0022, CMCTAG), CHOP (also known as DDIT3) (#2895, Cell Signaling Technology), XBP-1s (#12782, Cell Signaling Technology), BiP (also known as HSPA5) (#3177, Cell

Table 1. Primers Used for RT-PCR

Primers	Sequence
mCel-Fwd	5'-CGCCTGGAGGTTCTATTTCTTG-3'
mCel-Rev	5'-GCCCTTGAAGATGTCAACAGA-3'
hCEL/hCEL-HYB1-Fwd	5'-AAAAGGTGGCTGAGAAGGTGG-3'
hCEL/hCEL-HYB1-Rev	5'-CATCAATGACAGGGACGAAGC-3'
Ddit3-Fwd	5'-GAACCTGAGGAGAGAGTGTTCC-3'
Ddit3-Rev	5'-AGGGACTCAGCTGCCATGAC-3'
Hspa5-Fwd	5'-ACTTGGGGACCACCTATTCCT-3'
Hspa5-Rev	5'-GTTGCCCTGATCGTTGGCTA-3'
Hspa1a-Fwd	5'-ATGGTGCAGTCCGACATGAAG-3'
Hspa1a-Rev	5'-GCTGAGAGTCGTTGAAGTAGGC-3'
Hsp90aa1-Fwd	5'-TGTTGCGGTACTACACATCTGC-3'
Hsp90aa1-Rev	5'-GTCCTTGGTCTCACCTGTGATA-3'
Hsp90ab1-Fwd	5'-GTCCGCCGTGTGTTCATCAT-3'
Hsp90ab1-Rev	5'-GCACTTCTTGACGATGTTCTTGC-3'
Atf4-Fwd	5'-CTTGGCCAGTGCCTCAGACA-3'
Atf4-Rev	5'-CATGGTTTCCAGGTCATCCA-3'
Tnf-Fwd	5'-CCAAAGGGATGAGAAGTTCC-3'
Tnf-Rev	5'-CTCCACTTGGTGGTTTGCTA-3'
Il6-Fwd	5'-AGTTGCCTTCTTGGGACTGA-3'
Il6-Rev	5'-TCCACGATTTCCCAGAGAAC-3'
Bcl2-Fwd	5'-GTCGCTACCGTCGTGACTTC-3'
Bcl2-Rev	5'-CAGACATGCACCTACCCAGC-3'
Acta2-Fwd	5'-GCCAGTCGCTGTCAGGAACCC-3'
Acta2-Rev	5'-CCAGCGAAGCCGGCCTTACA-3'
Gapdh-Fwd	5'-AGGTCGGTGTGAACGGATTTG-3'
Gapdh-Rev	5'-TGTAGACCATGTAGTTGAGGTCA-3'

Signaling Technology), Beclin1 (11306-1-AP, Proteintech), P62 (#39749, Cell Signaling Technology), LC3 (#12741, Cell Signaling Technology), β-actin (66009-1-Ig, Proteintech) and secondary antibodies (anti-mouse IgG SA00001-1 or anti-rabbit IgG SA00001-2, Proteintech). Immunoblotting analysis of CEL proteins in different fractions of transfected HEK293T cells was performed with another antibody against CEL (HPA052701, Sigma). Densitometric analysis was carried out using Image J software.

Quantitative Reverse Transcriptase Polymerase Chain Reaction

Total RNA was extracted using TRIzol reagent (Invitrogen), and then 1 μg total RNA was reverse transcribed into cDNA using the RevertAid First Strand cDNA Synthesis Kit (Takara, 036A). qRT-PCR was performed on a Light Cycler 480 II System (Roche, Sandhofer) using Hieff UNICON qPCR SYBR Green Master Mix (YEASEN Biotechnology) as per the manufacturer's instructions. To assess *hCEL* and *hCEL-HYB1* mRNA expression levels, we designed a specific primer pair according to the common sequence of *hCEL* and *hCEL-HYB1*, which was capable of amplifying the mRNA of *hCEL* and *hCEL-HYB1* efficiently. The murine *Gapdh* gene was used as an internal RNA loading control.

Primers used in this study are listed in Table 1. Relative mRNA expression levels were calculated using the 2-ΔΔCT method. Except for the assessment of *CEL* mRNA expression, results were expressed as fold changes compared with wild-type.

Transmission Electron Microscopy

Pancreatic tissues were cut in 1mm pieces and removed to an Eppendorf tube with fresh transmission electron microscopy fixative (P1126, Solarbio). The tissues were post-fixed with 1% OsO_4 in 0.1 M phosphate buffer (pH 7.4) for 2 hours at room temperature in the dark. After removal of OsO_4, the tissues were rinsed in 0.1 M phosphate buffer (pH 7.4) 3 times, for 15 minutes each time. Subsequently, the tissues were dehydrated in grades of alcohol (30%-100%) at room temperature. The samples were then placed in propylene oxide for 1 hour and infiltrated overnight with a 1:1 mixture of propylene oxide and EMBed 812. The embedding models with resin and samples were placed in a 60 °C oven to polymerize for 48 hours. Ultrathin sections (50 nm) were cut on an ultra-microtome (Leica, Leica UC7), transferred to 150 mesh copper grids, stained with lead citrate, and examined in a Transmission Electron Microscope (Hitachi, HT7800).

Statistical Analysis

The data were analyzed using GraphPad Prism 6 and IBM SPSS 20.0 software. Results are expressed in terms of the means ± standard deviation. Differences of means between two groups were analyzed by a 2-tailed unpaired Student t test. One-way analysis of variance was used for multiple group comparisons, followed by Holms–Sidak post hoc pairwise multiple comparison. A P value of less than .05 was considered to be statistically significant.

References

1. Gardner TB, Adler DG, Forsmark CE, Sauer BG, Taylor JR, Whitcomb DC. ACG clinical guideline: chronic pancreatitis. Am J Gastroenterol 2020;115:322–339.

2. Chiari H. Über die Selbstverdauung des menschlichen Pankreas. Z Heilkunde 1896;17:69–96.

3. Hegyi E, Sahin-Tóth M. Genetic risk in chronic pancreatitis: the trypsin-dependent pathway. Dig Dis Sci 2017; 62:1692–1701.

4. Whitcomb DC, Gorry MC, Preston RA, Furey W, Sossenheimer MJ, Ulrich CD, Martin SP, Gates LK Jr, Amann ST, Toskes PP, Liddle R, McGrath K, Uomo G, Post JC, Ehrlich GD. Hereditary pancreatitis is caused by a mutation in the cationic trypsinogen gene. Nat Genet 1996;14:141–145.

5. Le Maréchal C, Masson E, Chen JM, Morel F, Ruszniewski P, Levy P, Férec C. Hereditary pancreatitis caused by triplication of the trypsinogen locus. Nat Genet 2006;38:1372–1374.

6. Huang H, Swidnicka-Siergiejko AK, Daniluk J, Gaiser S, Yao Y, Peng L, Zhang Y, Liu Y, Dong M, Zhan X, Wang H, Bi Y, Li Z, Ji B, Logsdon CD. Transgenic expression of PRSS1 R122H sensitizes mice to pancreatitis. Gastroenterology 2020;158:1072–1082.

7. Zou WB, Cooper DN, Masson E, Pu N, Liao Z, Férec C, Chen JM. Trypsinogen (PRSS1 and PRSS2) gene dosage correlates with pancreatitis risk across genetic and transgenic studies: a systematic review and reanalysis. Hum Genet 2022, Online ahead of print.

8. Witt H, Luck W, Hennies HC, Classen M, Kage A, Lass U, Landt O, Becker M. Mutations in the gene encoding the serine protease inhibitor, Kazal type 1 are associated with chronic pancreatitis. Nat Genet 2000;25:213–216.

9. Sun C, Liu M, An W, Mao X, Jiang H, Zou W, Wu H, Liao Z, Li Z. Heterozygous Spink1 c.194+2T>C mutant mice spontaneously develop chronic pancreatitis. Gut 2020;69:967–968.

10. Rosendahl J, Witt H, Szmola R, Bhatia E, Ozsvári B, Landt O, Schulz HU, Gress TM, Pfützer R, Löhr M, Kovacs P, Blüher M, Stumvoll M, Choudhuri G, Hegyi P, te Morsche RH, Drenth JP, Truninger K, Macek M Jr, Puhl G, Witt U, Schmidt H, Büning C, Ockenga J, Kage A, Groneberg DA, Nickel R, Berg T, Wiedenmann B, Bödeker H, Keim V, Mössner J, Teich N, Sahin-Tóth M. Chymotrypsin C (CTRC) variants that diminish activity or secretion are associated with chronic pancreatitis. Nat Genet 2008;40:78–82.

11. Rosendahl J, Kirsten H, Hegyi E, Kovacs P, Weiss FU, Laumen H, Lichtner P, Ruffert C, Chen JM, Masson E, Beer S, Zimmer C, Seltsam K, Algül H, Bühler F, Bruno MJ, Bugert P, Burkhardt R, Cavestro GM, Cichoz-Lach H, Farré A, Frank J, Gambaro G, Gimpfl S, Grallert H, Griesmann H, Grützmann R, Hellerbrand C, Hegyi P, Hollenbach M, Iordache S, Jurkowska G, Keim V, Kiefer F, Krug S, Landt O, Leo MD, Lerch MM, Lévy P, Löffler M, Löhr M, Ludwig M, Macek M, Malats N, Malecka-Panas E, Malerba G, Mann K, Mayerle J, Mohr S, Te Morsche RHM, Motyka M, Mueller S, Müller T, Nöthen MM, Pedrazzoli S, Pereira SP, Peters A, Pfützer R, Real FX, Rebours V, Ridinger M, Rietschel M, Rösmann E, Saftoiu A, Schneider A, Schulz HU, Soranzo N, Soyka M, Simon P, Skipworth J, Stickel F, Strauch K, Stumvoll M, Testoni PA, Tönjes A, Werner L, Werner J, Wodarz N, Ziegler M, Masamune A, Mössner J, Férec C, Michl P, Drenth J PH, Witt H, Scholz M, Sahin-Tóth M. all members of the PanEuropean Working group on ACP. Genome-wide association study identifies inversion in the CTRB1-CTRB2 locus to modify risk for alcoholic and non-alcoholic chronic pancreatitis. Gut 2018;67:1855–1863.

12. Tang XY, Zou WB, Masson E, Hu LH, Ferec C, Chen JM, Li ZS, Liao Z. The CTRB1-CTRB2 risk allele for chronic pancreatitis discovered in European populations does not contribute to disease risk variation in the Chinese population due to near allele fixation. Gut 2018; 67:1368–1369.

13. Witt H, Sahin-Tóth M, Landt O, Chen JM, Kähne T, Drenth JP, Kukor Z, Szepessy E, Halangk W, Dahm S, Rohde K, Schulz HU, Le Maréchal C, Akar N, Ammann RW, Truninger K, Bargetzi M, Bhatia E, Castellani C, Cavestro GM, Cerny M, Destro-Bisol G, Spedini G, Eiberg H, Jansen JB, Koudova M, Rausova E, Macek M Jr, Malats N, Real FX, Menzel HJ, Moral P, Galavotti R, Pignatti PF, Rickards O, Spicak J, Zarnescu NO, Böck W, Gress TM, Friess H, Ockenga J, Schmidt H, Pfützer R, Löhr M, Simon P, Weiss FU, Lerch MM, Teich N, Keim V, Berg T, Wiedenmann B, Luck W, Groneberg DA, Becker M, Keil T, Kage A, Bernardova J, Braun M, Güldner C, Halangk J, Rosendahl J, Witt U, Treiber M, Nickel R, Férec C. A degradation-sensitive anionic trypsinogen (PRSS2) variant protects against chronic pancreatitis. Nat Genet 2006;38:668–673.

14. Sahin-Tóth M. Genetic risk in chronic pancreatitis: the misfolding-dependent pathway. Curr Opin Gastroenterol 2017;33:390–395.

15. Mayerle J, Sendler M, Hegyi E, Beyer G, Lerch MM, Sahin-Tóth M. Genetics, cell biology, and pathophysiology of pancreatitis. Gastroenterology 2019; 156:1951–1968.e1.

16. Kereszturi E, Szmola R, Kukor Z, Simon P, Weiss FU, Lerch MM, Sahin-Tóth M. Hereditary pancreatitis caused by mutation-induced misfolding of human cationic trypsinogen: a novel disease mechanism. Hum Mutat 2009; 30:575–582.

17. Schnúr A, Beer S, Witt H, Hegyi P, Sahin-Tóth M. Functional effects of 13 rare PRSS1 variants presumed to cause chronic pancreatitis. Gut 2014;63:337–343.

18. Witt H, Beer S, Rosendahl J, Chen JM, Chandak GR, Masamune A, Bence M, Szmola R, Oracz G, Macek M Jr, Bhatia E, Steigenberger S, Lasher D, Bühler F,

Delaporte C, Tebbing J, Ludwig M, Pilsak C, Saum K, Bugert P, Masson E, Paliwal S, Bhaskar S, Sobczynska-Tomaszewska A, Bak D, Balascak I, Choudhuri G, Nageshwar Reddy D, Rao GV, Thomas V, Kume K, Nakano E, Kakuta Y, Shimosegawa T, Durko L, Szabó A, Schnúr A, Hegyi P, Rakonczay Z Jr, Pfützer R, Schneider A, Groneberg DA, Braun M, Schmidt H, Witt U, Friess H, Algül H, Landt O, Schuelke M, Krüger R, Wiedenmann B, Schmidt F, Zimmer KP, Kovacs P, Stumvoll M, Blüher M, Müller T, Janecke A, Teich N, Grützmann R, Schulz HU, Mössner J, Keim V, Löhr M, Férec C, Sahin-Tóth M. Variants in *CPA1* are strongly associated with early onset chronic pancreatitis. Nat Genet 2013;45:1216–1220.

19. Hegyi E, Sahin-Tóth M. Human *CPA1* mutation causes digestive enzyme misfolding and chronic pancreatitis in mice. Gut 2019;68:301–312.

20. Fjeld K, Weiss FU, Lasher D, Rosendahl J, Chen JM, Johansson BB, Kirsten H, Ruffert C, Masson E, Steine SJ, Bugert P, Cnop M, Grützmann R, Mayerle J, Mössner J, Ringdal M, Schulz HU, Sendler M, Simon P, Sztromwasser P, Torsvik J, Scholz M, Tjora E, Férec C, Witt H, Lerch MM, Njølstad PR, Johansson S, Molven A. A recombined allele of the lipase gene *CEL* and its pseudogene *CELP* confers susceptibility to chronic pancreatitis. Nat Genet 2015;47:518–522.

21. Zou WB, Boulling A, Masamune A, Issarapu P, Masson E, Wu H, Sun XT, Hu LH, Zhou DZ, He L, Fichou Y, Nakano E, Hamada S, Kakuta Y, Kume K, Isayama H, Paliwal S, Mani KR, Bhaskar S, Cooper DN, Férec C, Shimosegawa T, Chandak GR, Chen JM, Li ZS, Liao Z. No association between *CEL-HYB* hybrid allele and chronic pancreatitis in Asian populations. Gastroenterology 2016;150:1558–1560.e5.

22. Oracz G, Kujko AA, Fjeld K, Wertheim-Tysarowska K, Adamus-Białek W, Steine SJ, Koziel D, Gluszek S, Molven A, Rygiel AM. The hybrid allele 1 of carboxyl-ester lipase (*CEL-HYB1*) in Polish pediatric patients with chronic pancreatitis. Pancreatology 2019; 19:531–534.

23. Johansson BB, Fjeld K, El Jellas K, Gravdal A, Dalva M, Tjora E, Ræder H, Kulkarni RN, Johansson S, Njølstad PR, Molven A. The role of the carboxyl ester lipase (CEL) gene in pancreatic disease. Pancreatology 2018;18:12–19.

24. Mao XT, Deng SJ, Kang RL, Wang YC, Li ZS, Zou WB, Liao Z. Homozygosity of short VNTR lengths in the CEL gene may confer susceptibility to idiopathic chronic pancreatitis. Pancreatology 2021;21:1311–1316.

25. Raeder H, Johansson S, Holm PI, Haldorsen IS, Mas E, Sbarra V, Nermoen I, Eide SA, Grevle L, Bjørkhaug L, Sagen JV, Aksnes L, Søvik O, Lombardo D, Molven A, Njølstad PR. Mutations in the *CEL* VNTR cause a syndrome of diabetes and pancreatic exocrine dysfunction. Nat Genet 2006;38:54–62.

26. Cassidy BM, Zino S, Fjeld K, Molven A, Lowe ME, Xiao X. Single nucleotide polymorphisms in *CEL-HYB1* increase risk for chronic pancreatitis through proteotoxic misfolding. Hum Mutat 2020;41:1967–1978.

27. Dalva M, Lavik IK, El Jellas K, Gravdal A, Lugea A, Pandol SJ, Njølstad PR, Waldron RT, Fjeld K, Johansson BB, Molven A. Pathogenic carboxyl ester lipase (CEL) variants interact with the normal CEL protein in pancreatic cells. Cells 2020;9:244.

28. Vesterhus M, Raeder H, Kurpad AJ, Kawamori D, Molven A, Kulkarni RN, Kahn CR, Njølstad PR. Pancreatic function in carboxyl-ester lipase knockout mice. Pancreatology 2010;10:467–476.

29. Holmes RS, Cox LA. Comparative structures and evolution of vertebrate carboxyl ester lipase (*CEL*) genes and proteins with a major role in reverse cholesterol transport. Cholesterol 2011;2011:781643.

30. Gravdal A, Xiao X, Cnop M, El Jellas K, Johansson S, Njølstad PR, Lowe ME, Johansson BB, Molven A, Fjeld K. The position of single-base deletions in the VNTR sequence of the carboxyl ester lipase (*CEL*) gene determines proteotoxicity. J Biol Chem 2021;296:100661.

31. Tjora E, Gravdal A, Engjom T, Cnop M, Johansson BB, Dimcevski GG, Molven A, Fjeld K. Protein misfolding in combination with other risk factors in *CEL-HYB1*-mediated chronic pancreatitis. Eur J Gastroenterol Hepatol 2021;33:839–843.

32. Xiao X, Jones G, Sevilla WA, Stolz DB, Magee KE, Haughney M, Mukherjee A, Wang Y, Lowe ME. A carboxyl ester lipase (CEL) mutant causes chronic pancreatitis by forming intracellular aggregates that activate apoptosis. J Biol Chem 2016;291:23224–23236.

33. Lansbury PT Jr. Evolution of amyloid: what normal protein folding may tell us about fibrillogenesis and disease. Proc Natl Acad Sci U S A 1999;96:3342–3344.

34. Diakopoulos KN, Lesina M, Wörmann S, Song L, Aichler M, Schild L, Artati A, Römisch-Margl W, Wartmann T, Fischer R, Kabiri Y, Zischka H, Halangk W, Demir IE, Pilsak C, Walch A, Mantzoros CS, Steiner JM, Erkan M, Schmid RM, Witt H, Adamski J, Algül H. Impaired autophagy induces chronic atrophic pancreatitis in mice via sex- and nutrition-dependent processes. Gastroenterology 2015;148:626–638.e17.

35. Saluja A, Dudeja V, Dawra R, Sah RP. Early intra-acinar events in pathogenesis of pancreatitis. Gastroenterology 2019;156:1979–1993.

36. Molven A, Fjeld K, Lowe ME. Lipase genetic variants in chronic pancreatitis: when the end is wrong, all's not well. Gastroenterology 2016;150:1515–1518.

37. Ræder H, Vesterhus M, El Ouaamari A, Paulo JA, McAllister FE, Liew CW, Hu J, Kawamori D, Molven A, Gygi SP, Njølstad PR, Kahn CR, Kulkarni RN. Absence of diabetes and pancreatic exocrine dysfunction in a transgenic model of carboxyl-ester lipase-MODY (maturity-onset diabetes of the young). PLoS One 2013; 8:e60229.

38. Wildi S, Kleeff J, Mayerle J, Zimmermann A, Böttinger EP, Wakefield L, Büchler MW, Friess H, Korc M. Suppression of transforming growth factor beta signalling aborts caerulein induced pancreatitis and eliminates restricted stimulation at high caerulein concentrations. Gut 2007;56:685–692.

39. Zhang GX, Wang MX, Nie W, Liu DW, Zhang Y, Liu HB. P2X7R blockade prevents NLRP3 inflammasome

activation and pancreatic fibrosis in a mouse model of chronic pancreatitis. Pancreas 2017;46:1327–1335.

Correspondence
Address correspondence to: Zhuan Liao, Department of Gastroenterology, Changhai Hospital, The Second Military Medical University, 168 Changhai Road, Shanghai 200433, China. e-mail: liaozhuan@smmu.edu.cn; tel: 0086-21-31161004; fax: 0086-21-55621735. Wen-Bin Zou, Department of Gastroenterology, Changhai Hospital, The Second Military Medical University, 168 Changhai Road, Shanghai 200433, China. e-mail: dr.wenbinzou@hotmail.com; tel: 0086-21-31161353; fax: 0086-21-55621735.

Conflicts of interest
The authors disclose no conflicts.